Computational characterisation of microwave heating of fibre preforms for CVI of SiCf/SiC composites

Porter, Matthew T.; Binner, Jon; Cinibulk, Michael K.; Stern, Kevin E.; Yakovlev, Vadim V.

DOI:
10.1016/j.jeurceramsoc.2022.12.035

Document Version
Publisher's PDF, also known as Version of record

Citation for published version (Harvard):
Porter, MT, Binner, J, Cinibulk, MK, Stern, KE & Yakovlev, VV 2023, 'Computational characterisation of microwave heating of fibre preforms for CVI of SiCf/SiC composites', *Journal of the European Ceramic Society*, vol. 43, no. 5, pp. 1808-1827. https://doi.org/10.1016/j.jeurceramsoc.2022.12.035

Journal of the European Ceramic Society 43 (2023) 1808–1827

Contents lists available at ScienceDirect

Journal of the European Ceramic Society

journal homepage: www.elsevier.com/locate/jeurceramsoc

Computational characterisation of microwave heating of fibre preforms for CVI of SiC_f/SiC composites

Matthew T. Porter [a,*], Jon Binner [a], Michael K. Cinibulk [b], Kevin E. Stern [c], Vadim V. Yakovlev [c,*]

[a] School of Metallurgy and Materials, University of Birmingham, Edgbaston, Birmingham B15 2TT, UK
[b] Materials and Manufacturing Directorate, Air Force Research Laboratory, WPAFB, OH 45433, USA
[c] Department of Mathematical Sciences, Worcester Polytechnic Institute, Worcester, MA 01609, USA

ARTICLE INFO

Keywords:
Chemical vapour infiltration
Microwave-assisted processing
SiC_f/SiC composites
Multiphysics simulation
CMC

ABSTRACT

Silicon carbide fibre reinforced silicon carbide matrix composites (SiC_f/SiC) are known as materials with high-performance mechanical properties for the aerospace industry. Microwave-enhanced (ME) chemical vapour infiltration (CVI) heating of ceramic matrix composites is potentially an energy efficient production technique capable of yielding near fully dense SiC_f/SiC composites in a much shorter time span. This paper reports on the output of computational analysis of electromagnetic (EM) and thermal characteristics of the ME CVI process occurring with thin circular SiC fibre preform in a Labotron microwave system from SAIREM. Computer simulation is performed with the use of the finite-difference time-domain technique implemented in QuickWave computational environment. Multiple puzzling phenomena observed in the earlier experimental work are illuminated in the present study and the causes for the formation of microwave-induced temperature fields are clarified. With the use of the developed EM model, resonant and non-resonant frequencies of the Labotron system for different temperatures of the processed samples are analysed to explain the differences and variability in heating rates. This showed that when microwave processing of small SiC samples, energy coupling is extremely sensitive to frequency: a change of the reflection coefficient from 0.05 (absorbing) to 0.75 (reflective) could be made by a drift as small as 0.003–0.005 GHz, respectively, indicating the importance of scaling the microwave cavity to the sample size and the ability to precisely control the frequency of the microwave source. Moreover, energy coupling is temperature-dependent: low reflections produces very high heating rates (greater than 550 °C min^{-1}); the opposite is true for high reflections where heating rates are significantly slower. Temperature fields in the SiC fibre preforms are computed with the coupled EM-thermal model at different frequencies. It is shown that while being highly non-uniform in the beginning of the process, temperature patterns evolve to being fairly homogeneous by its end. Overall, the results suggest a means for better control of the equipment to pave the way to more efficient, controlled, and repeatable implementations of the ME CVI technology to produce high quality SiC_f/SiC composites.

1. Introduction

The relatively recent widespread utilisation of composites materials is perhaps best exemplified by the aerospace industry. Their uncompromising properties are of utmost importance [1] providing high strength, low mass and high stiffness. To this end, they have seen a recent explosion in the industry as manufacturing has become more advanced and significantly cheaper. This development is now expanding further into turbo-fan engines as ceramic matrix composites properties are of significant interest to this industry.

Ceramic matrix composites (CMC), specifically silicon carbide fibre reinforced silicon carbide matrix composites (SiC_f/SiC), have been recognised as an aspirant material for these applications [2–7]. They are of significant interest due to the superior characteristics composite materials have over the monolithic equivalents [8]. The application of SiC_f/SiC in the aerospace industry is increasing, replacing Ni-Ti super-alloy components, and enabling engines to operate at higher temperatures leading to a reduced active cooling requirement and enhanced thermal performance [9]. Excellent high-temperature specific strength properties mean that the size and mass of the engines can be reduced, which is expected to reduce specific fuel consumption by up to 25% [10] and improve the propulsive, thermal and transfer efficiencies.

* Corresponding authors.
E-mail addresses: mtporter224@gmail.com (M.T. Porter), vadim@wpi.edu (V.V. Yakovlev).

https://doi.org/10.1016/j.jeurceramsoc.2022.12.035
Received 26 May 2022; Received in revised form 12 December 2022; Accepted 15 December 2022
Available online 19 December 2022

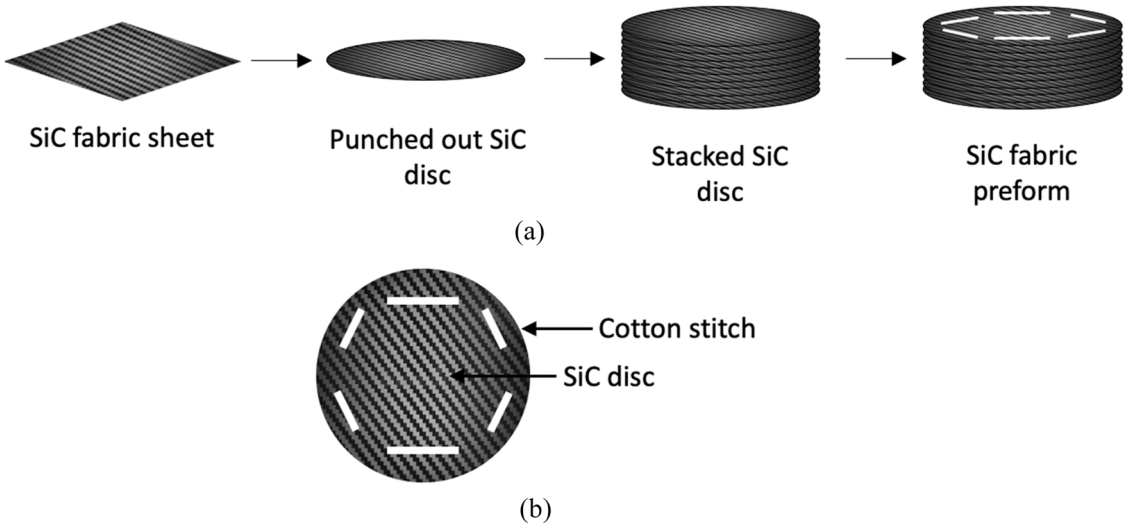

Fig. 1. Fabrication route for a SiC_f/SiC composite preform used in this work (a), and a planar view of the stitched SiC_f preform (b).

Currently, three advanced manufacturing methods are of particular interest to industry; reactive melt infiltration (RMI), polymer infiltration and pyrolysis (PIP) and chemical vapour infiltration (CVI) [11,12], which all have their advantages and disadvantages. RMI can produce dense CMCs quickly, but microstructures can contain residual silicon phases and the molten metals can damage the fibres and limit applications to below the melting temperature. PIP requires that the infiltration step is undertaken multiple times, up to a dozen, whilst the matrices produced can have a pre-cracked microstructure due to the high shrinkage of the precursor material during firing. In contrast, CVI can create an extremely refined microstructure with little or no preform degradation and minimal residual stresses [13,14], however it has three major challenges:

(i) Conventional processing uses isothermal heating rates, which are of necessity extremely slow.
(ii) Premature pore closure results in a need for repeated machining stages to re-open the closed channels, which reduces precursor conversion efficiency to $< 5\%$ [8].
(iii) Because of the previous two points, manufacturing speeds are very slow, typically 2–3 months, and associated costs are very high – and hence so is the resulting product.

CVI is the process of infiltrating a porous matrix of typically continuous fibres (a preform) with a mixture of precursor gases that react, decompose and precipitate a solid matrix at high temperature. The primary objective of CVI, like the other advanced manufacturing methods mentioned, is to increase the density of the porous preform to as close to the theoretical density as possible [15]. Due to the complexity of achieving dense CMCs several variants of CVI techniques have developed over time that can be crudely classified by:

(1) temperature,
(2) pressure, and
(3) heating method.

Focusing on the latter, microwave-enhanced CVI (ME CVI) has been proposed as a potential solution to heat the SiC fibre preform for CVI [9,16–18]. It produces a favourable inverse temperature profile, meaning the temperature is hottest at the centre of the component in contrast to conventional CVI. This inverted profile means densification initiates within the sample, therefore avoiding surface porosity closure. It has recently been shown that this method has the potential to yield near fully dense SiC_f/SiC composites in a substantially shorter time span [19]. This research has demonstrated proof of the concept that the inverse densification profile can be controlled and the resulting SiC deposit can have a close to stoichiometric composition as well as a highly crystalline microstructure. It also showed that this process achieved a 25% increase in density in only 8 h and that full densification is predicted to be achievable in about 100 h [19,20] compared with weeks or months for conventional CVI [15].

However, despite successful demonstration of the benefits of this technology, the most recent advancements in ME CVI have highlighted several unexplained experimental observations. The principal of them was a lack of reproducibility of samples due to inconsistent power absorption. This has exposed the difficulties in controlling microwave heating of the SiC fabric preform. Without reasonable explanations and subsequent mitigations for these complications, it is possible that the development of the ME CVI process much beyond lab scale manufacturing will be impeded significantly.

Substantial research resources are required to resolve the issues associated with microwave processing of CMCs and fully exploit this novel processing technique. To facilitate this, an improved understanding of material-microwave interactions, temperature control, and extreme thermal gradients is required [21], all of which could also yield benefits to the ceramics and wider materials science communities [22–25]. Improved thermal management of materials during microwave processing could provide enhanced microstructures with heightened or even unprecedented properties. All this could lead to new industry perceptions and more efficient processing, contributing ultimately to more environmentally responsible manufacturing [26].

This paper presents the results of computational analysis of electromagnetic (EM) and thermal characteristics of the ME CVI process carried out with thin (thickness h from 8 to 24 mm) circular SiC fibre preform (diameter d from 55 to 165 mm) in a Labotron microwave system from SAIREM. The multiple unexplained observations in the experimental work [19,20] have been explained using computer simulations, which have clarified the causes for the formation of microwave-induced temperature fields. With the use of the developed EM model, resonant and non-resonant frequencies of the experimental system for different temperatures of the processed SiC_f/SiC samples were analysed to explain the differences and variability in heating rates. 3D temperature fields in the SiC fibre preforms were also computed (with the coupled EM-thermal model) at different frequencies and showed, while being highly non-uniform in the beginning of the process, temperature patterns evolve to being quite homogeneous by its end. The results suggest a means for better control of the equipment to pave the way to more efficient, controlled, and repeatable implementations of the ME CVI

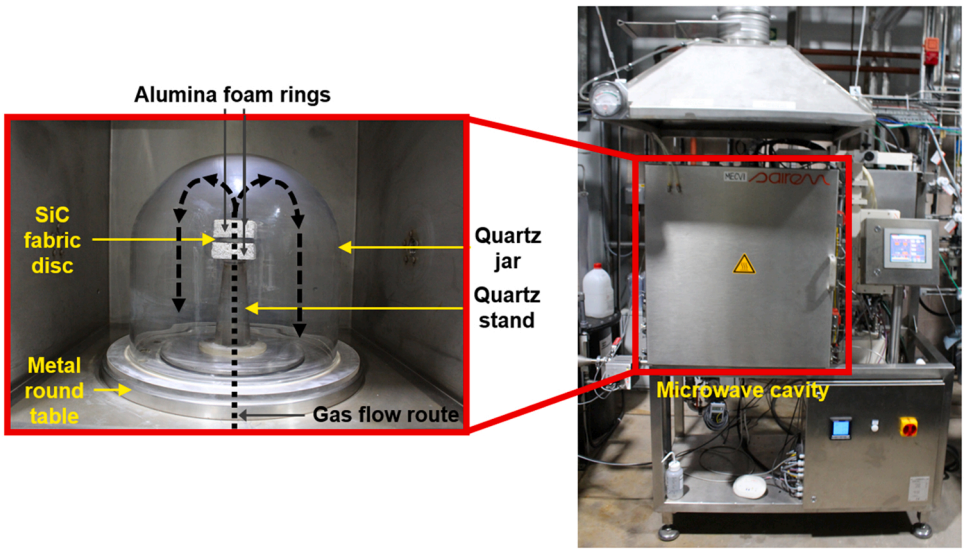

Fig. 2. Labotron HTE M30KLB Pro by SAIREM: A general view of the microwave system (right) and the interior of the cavity showing the experimental arrangement (left).

technology to produce high quality SiC_f/SiC composites.

2. Experimental studies

2.1. SiC fibre and preform

Preforms for the ME CVI process were prepared by layering up SiC fabric plies (Hi Nicalon Type-S, third generation fibres from COI Ceramics, Inc., CA, USA) one on top of another, Fig. 1. Typically, 20 disc-shaped plies were used to create each sample, the discs were produced using a 55 mm diameter wad punch to cut the discs from the cloth. The stamped-out layers were aligned and stitched by hand using a fine cotton thread to hold the plies together; the resulting stacked fabric discs had 80 ± 5% porosity. This was determined by measuring the mass of the assembled fabric preform without stitching, once stitched measuring the height of the stack and calculating the volume of the preform to determine the actual density. The relative density was then determined by dividing actual density of fabric preform by the theoretical density of a 100% dense Hi Nicalon Type-S preform (3.1 g cm^{-3}), the porosity was then calculated by subtracting this relative density as a percentage from 100.

Differences between samples in terms of porosity were attribute to variation in the hand stitching. A 25 vol% SiC slurry was painted around the circumference of each assembled preform[1] to shield any sharp points (e.g., protruding fibres) from the electric field, otherwise the local field would be enhanced, and electrical discharges occur. Deposition of SiC into the pores of the SiC preform was realised by decomposition of gaseous methyltrichlorosilane (MTS) in hydrogen:

$$CH_3SiCl_{3(g)} + (n)H_{2(g)} \rightarrow SiC_{(s)} + 3HCl_{(g)} + H_{2(g)}$$

2.2. Microwave CVI equipment

The customised microwave oven (Labotron HTE M30KB CL PRO, SAIREM, France) included a microwave generator, a control unit and a 316 L polished stainless-steel rectangular cavity. The microwave generator (Muegge Electronics GmbH, Germany) employed a magnetron operated at a frequency of 2.45 ± 0.05 GHz and had a maximum power output of 3.0 kW that could be adjusted in 0.01 kW increments. The microwaves produced by the magnetron were modulated by a manual E/H tuner (SAIREM, France) and a four-stub auto tuner (SAIREM, France). Their combined use aimed to minimise the reflected power within the cavity and optimise the impedance matching, coupling and subsequent heating of the SiC samples. A secondary role was to protect the magnetron from extremes of reflective power that might result in overheating and shutdown.

The generator operated in controlled pulse mode to maintain the desired temperature, where the PID controller switched off the microwave generator when the pyrometer detected the set point temperature. This made the sample cool down approximately 20 °C before the controller switched the generator back on to increase the temperature. The cavity, waveguide and metal turntable (with an adjustable rotation speed) were also water-cooled to below 50 ℃; this improved the efficiency of microwave generation and prevented the thermal expansion of the components, which could have affected the microwave frequency of the system.

The quartz jar was the reaction vessel that protected the cavity's and waveguide's walls from the highly corrosive reactants and by-products of the decomposition reaction, the bottom wall and turntable were not protected. The hollow quartz stand was the entry point of the gas and supported the sample, which was placed between two alumina foam rings. The photos of the experimental system and the interior of the cavity are shown in Fig. 2.

2.3. Temperature control

Measuring and controlling the temperature was a critical element of the ME CVI process and was carried out using three contactless pyrometers that were integrated into the Labotron.

system. A single-colour pyrometer (1CP) (thermoMETER CTM3, Micro-Epsilon, NC, USA) was positioned in the top of the cavity and monitored the surface temperature of the SiC fibre preform up to 750 ℃; 0.9 was used as the emissivity value of SiC [27]. Two two-colour pyrometers (2CP) (thermoMETER CT ratio M1, Micro-Epsilon, NC, USA) were also used to measure the side and bottom surface temperatures of the SiC fabric preform, Fig. 3. The pyrometers used had a response time of 5 ms and an accuracy of ± 0.5% of the measured temperature; their working range was 700–1800 ℃. The bottom pyrometer controlled the

[1] CVI of the preforms could be undertaken either as made or following impregnation with SiC particles via the incorporation of a slurry followed by drying. This modelling work focused on unimpregnated preforms.

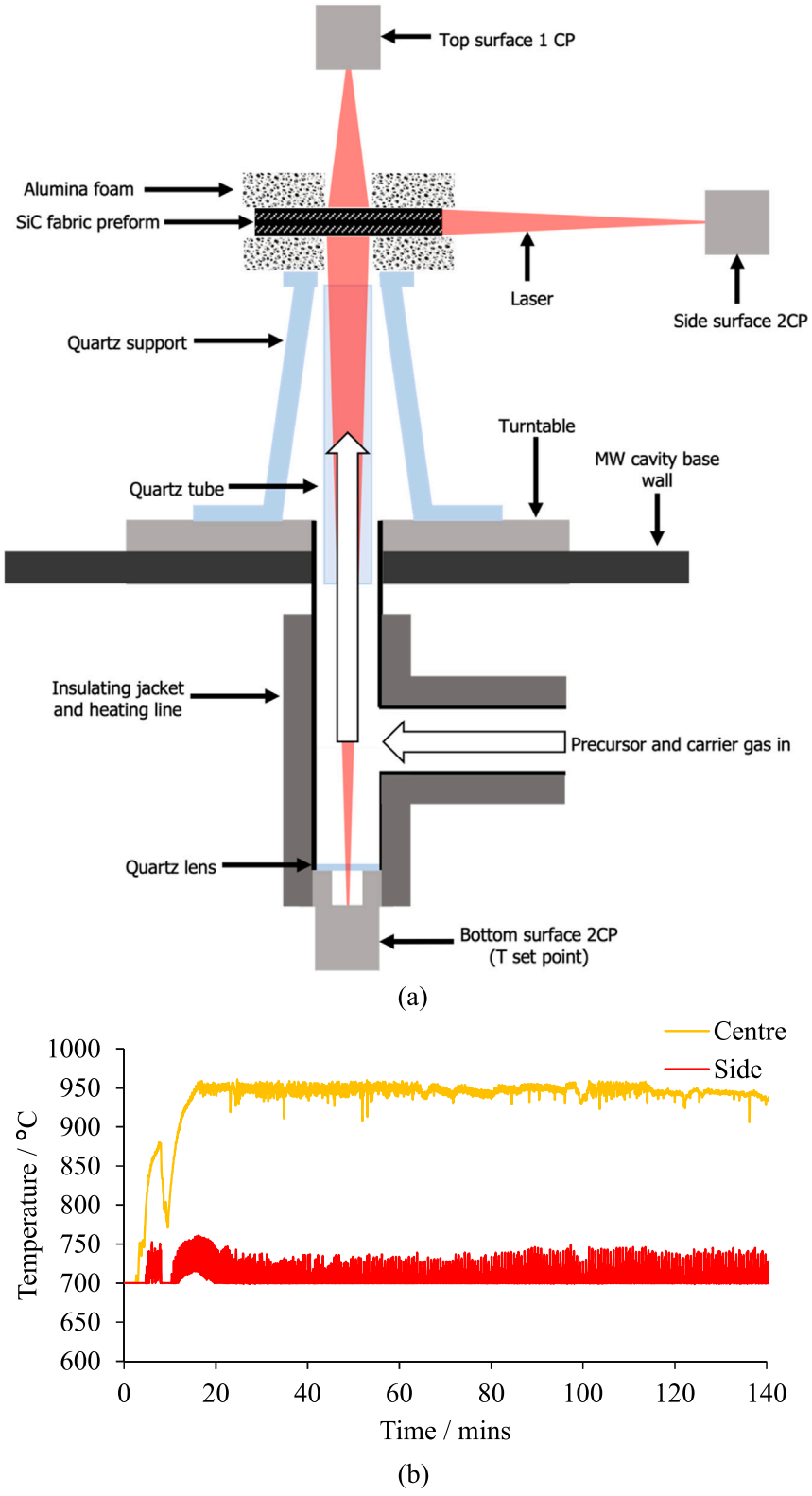

Fig. 3. A cross-sectional view of the temperature control arrangement of the pyrometers, sample and gas flows (a) and data showing the side pyrometer temperature measuring the SiC slurry coated edge and bottom pyrometer temperature with a set point at 950 °C measuring the SiC fabric temperature (b).

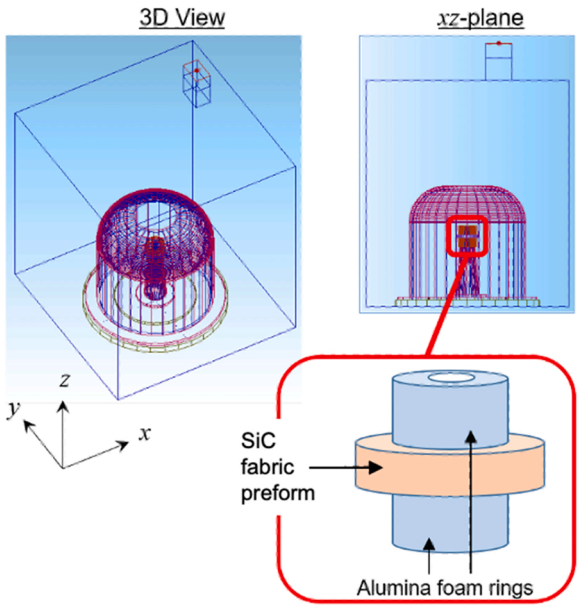

Fig. 4. 3D (left) and 2D (right) views of the SAIREM Labotron system in the model; rectangular cavity, feeding waveguide (on the top, non-centred), metal roundtable at the bottom, bell quartz jar, quartz support and the SiC fabric preform sandwiched by the alumina foam rings in the centre.

than the radius of the discs as well as the centre being better insulated. This further emphasises the need for a simulation tool to provide a more accurate understanding of this gradient. An upper-temperature limit of 1400 ℃ was set for safety purposes to prevent thermal runaway. The pyrometer was also never in direct contact with the gas stream that came up through the quartz stand and was heated to prevent MTS condensing on the quartz lens.

The experimentation, however, was not without issues – several unexplained observed phenomena made testing complex. One of these was a frequent change in heating rate whilst the input power was being kept constant; this made temperature control difficult despite the PID control, which was further exacerbated by density and permittivity changes that occurred during densification. Other experimental variables also investigated to understand the processing parameters included infiltration pressure, reactant gas ratio and reactant gas flow rate [20]. It was difficult to determine the direct effect, if any, that these other variables had on the heating of the SiC fabric preform due to the significant variability between samples that have already been described. However, anecdotally, decreasing the infiltration chamber pressure to < 300 mbar made heating the sample even more volatile, in part due to arcing between SiC fibres in the preform [28]. Furthermore, increasing the total gas flow rate appeared to have some convective cooling effect on the underside of the fabric preform where the pyrometer was measuring (see Fig. 3). All these factors contributed to a lack of reproducibility between virtually identical samples making comparisons between tests difficult. Furthermore, the microwave, hazardous gas and high temperature environment limited process control variations that could otherwise have been used to validate other test results. The reasons all indicated the need for an adequate computer simulation that could provide valuable insight into the process that could not be garnered experimentally.

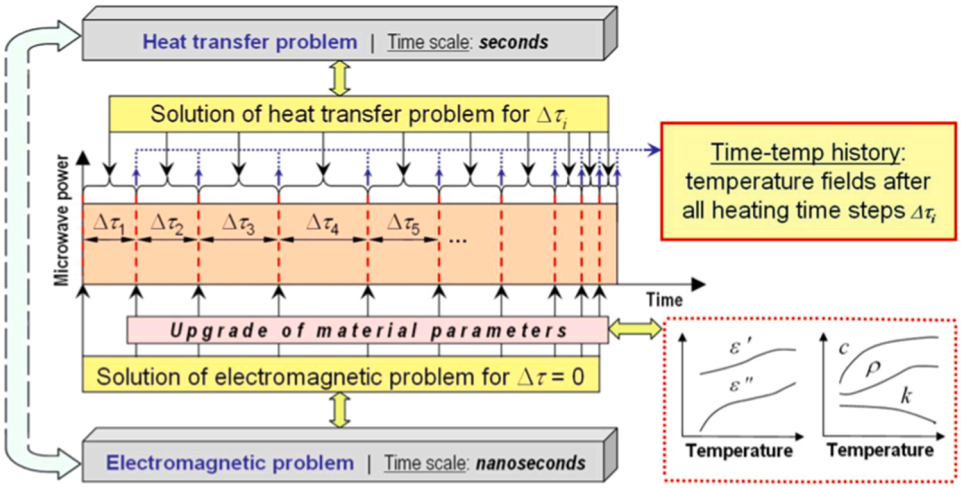

Fig. 5. Schematic representation of the iterative method computing microwave-induced temperature field evolving in time during microwave heating; the procedure was implemented with *QW* and *QW-BHM* [29–33].

set-point temperature via a feedback loop by modulating the power supplied to the cavity with the help of a PID controller. This kept the sample as close to the set-point temperature as possible, which was typically ± 15 ℃. Typically, the temperature difference between the bottom pyrometer and the side ranged between 200 and 250 °C[2] when the set point was between 900 and 1000 °C. It was assumed, due to the inability to physically measure the internal temperature of the sample, that the temperature observed on the lower surface was always lower than the actual temperature in the centre due to the thermal gradient in the vertical direction caused by increase heat loss at the surface. This gradient was expected to be at least order of magnitude less than the horizontal gradient due to height of the samples being significantly less

3. Simulation of microwave heating of SiC fibre preform

3.1. Computational approach

ME CVI is a complex phenomenon involving multiple interacting physical and chemical processes, so mimicking them all in a unified multiphysics model would have been very difficult and consequently was not in the scope of this work. The modelling objective was to single out the interaction of the heated SiC fibre preform with the microwaves and analyse the mechanisms of formation of the initial microwave-

[2] Note that side temperature measured is the surface of the slurry coated edge of the stacked fabric preform, which is not considered in the simulation.

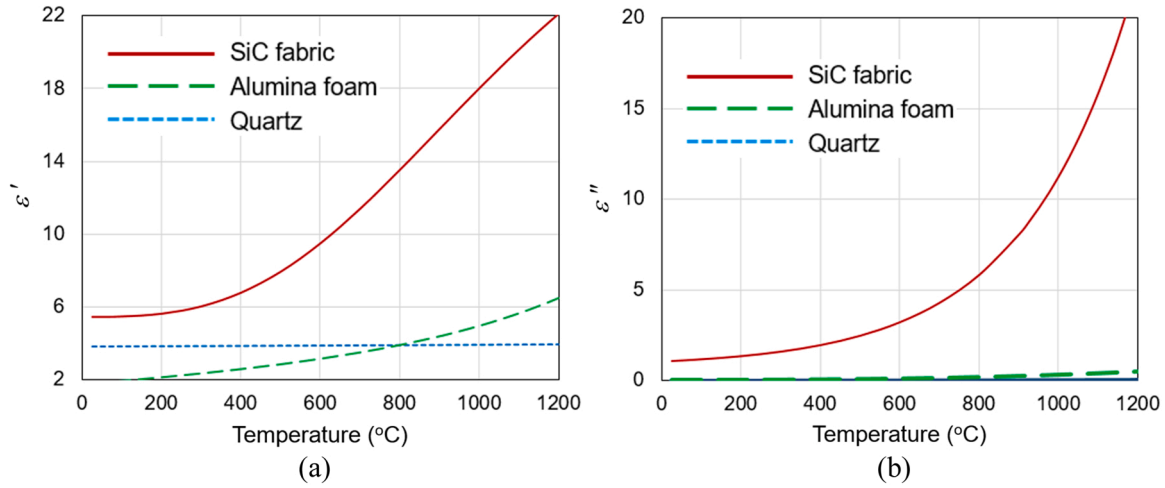

Fig. 6. Temperature-dependent complex permittivity of the three materials (SiC fabric preform, alumina foam and quartz) involved in the microwave processing: dielectric constant ε' (a) and the loss factor ε'' (b).

Table 1
Density of the materials used in the ME CVI process.

Material	Density (g/cm^3)
SiC fabric preform	0.48
Alumina foam	0.49
Quartz	2.2

induced temperature fields in the experimental system. Note that the simulation did not include the effects of SiC deposition, but primarily investigated the heating of just fibre preform.

Computer simulation of the EM and temperature fields associated with the ME CVI process was carried out with the help of a model developed of the Labotron HTE M30KB CL Pro system cavity containing a SiC fabric preform sample. Simulations were done for the SiC fibre preform of three sizes, *A* ($d = 55$ mm, $h = 8$ mm), *B* ($d = 110$ mm, $h = 16$ mm), and *C* ($d = 165$ mm, $h = 24$ mm) in the 550 × 550 x 610 mm metal cavity.

The internal structure of the cavity was reproduced, in a fully parameterised form, in a 3D model to be used in the environment of the 3D Finite-Difference Time-Domain (FDTD) electromagnetic simulator *QuickWave*™ [29] that included the thermal solver *QW-Basic Heating Module (BHM)* ™ simulating microwave-induced heat transfer on the same mesh [29]. The FDTD technique solves Maxwell's equations with standard boundary conditions for the electric and magnetic fields on the outer walls of the metal cavity and on all interfaces between the dielectric media involved. The internal layout of the cavity, and all the material components reproduced in the model, are shown in Fig. 4.

The method used was established by [30–33] for solving an EM-thermal two-way coupling problem via an iterative solution. This approach relied on nine-order-magnitude difference in the time scales of the EM and thermal problems and data on temperature-dependent EM and thermal material properties – complex permittivity $\varepsilon = \varepsilon' - j\varepsilon''$ (where ε' is dielectric constant and ε'' is the loss factor), density ρ, specific heat capacity C_p and thermal conductivity k. The EM and thermal solvers operate in tandem as parts of a computational procedure, schematically outlined in Fig. 5, in which a steady state solution of the EM problem became an input for the thermal problem, whose output presented the temperature field induced within the heated material after the pre-set heating time step (HTS), $\Delta\tau$. In the repeated runs of the solvers, the material parameters were upgraded in every FDTD cell in accordance with the temperature distributions determined after each EM-thermal iteration.

The key advantage of this method of coupling the EM and thermal processes in a unified model was that they were both simulated by the same numerical method over the same mesh. The HTS was a delicate

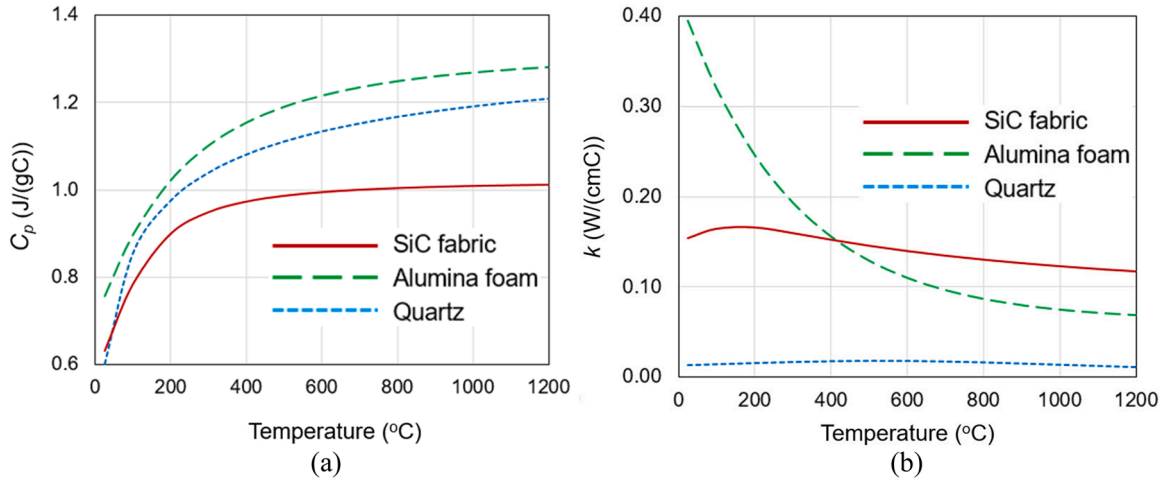

Fig. 7. Temperature-dependent specific heat (a) and thermal conductivity (b) of the three materials (SiC fabric, alumina foam and quartz) involved in the heating process.

Table 2
Details of the non-uniform mesh in the FDTD model.

SiC fabric preform		A: $d = 55$ mm, $h = 8$ mm	B: $d = 110$ mm, $h = 16$ mm	C: $d = 165$ mm, $h = 24$ mm
Max. cell size	… in air	8.0 mm		
	… in quartz[a]	4.5 mm		
	… in Al_2O_3[b]	2.0 mm[c]		
	… in SiC fabric preform[d]			
Min. cell size	… in *x*-direction	1.25 mm	1.5 mm	1.67 mm
	… in *y*-direction			
	… in *z*-direction	1.92 mm	1.0 mm	1.60 mm
Total number of cells in the model		2.2 mil	2.7 mil	3.7 mil
RAM		211 MB	272 MB	349 MB

[a] $\varepsilon'_{max} = 3.95$
[b] $\varepsilon'_{max} = 7.69$
[c] In alumina foam: 22 cells/wavelength; in SiC fabric: 13 cells/wavelength
[d] $\varepsilon'_{max} = 22.1$

point for this computational scheme, however, because it had to be assumed that during it the EM field did not change whilst the temperature-dependent material parameters did change. As long as the material properties varied linearly, $\Delta\tau$ could be chosen arbitrarily because any change in temperature determined by the thermal solver after its next run resulted in a correct update of ε' and ε'' for the EM simulation in the next iteration. With non-linear input data, the HTS needed to be small enough to make the increase in temperature sufficiently small to ensure an accurate upgrade of material parameters (and hence achieve a more precise simulation).

How the accuracy of the resulting iterative solution for microwave heating processes reaching very high temperatures depends on the HTS is not sufficiently studied in the literature. Thus for this work, a series of computational tests were undertaken (that are discuss in some detail in the Appendix) designed to check the behaviour of the time-temperature characteristics for different values of $\Delta\tau$. The results suggested that the $T_{max}(t)$ curves converged down to those corresponding to HTS values of 0.5 s and 5 s for the processes with high and low heating rates, respectively. These values were therefore used in this study to simulate the time evolutions of the microwave-induced temperature fields.

The EM boundary conditions applied to the cavity assumed that the 316 L stainless steel walls were theoretically perfectly (infinitively) conductive. In numerical simulation in the *QuickWave* computational environment, the electric conductivity of the walls was set, in accordance with a traditional computational convention, to a very high but finite number (10^7 Sm^{-1}). In the Labotron the M30KB CL Pro, the value of σ of this type of steel may be somewhat lower. However, based on the results in [34], it is believed that the slight difference in conductivity of the cavity will make no notable effect on the EM characteristics of the modelled system. Neumann (thermal insulation) boundary conditions were applied to all the surfaces of the SiC preform and Robin (convective) conditions (with the convection exchange coefficient being 5 $Wm^{-2}K^{-1}$ [35]) applied where the SiC fibre preform and alumina rings interfaced. Due to limitations of the QW BHM, a radiation boundary condition could not be applied to the surface of the disc as well. If it were possible, the radiation from the side of the disc would have enhanced the inverse temperature profile.

Table 3
Temperatures at which complex permittivity of the materials in the ME CVI process were chosen in simulation of frequency characteristics of the reflection coefficient (see Figs. 9 and 10).

Temperature (…) as a parameter in EM simulations /°C	The EM model uses material parameters of…		
	SiC fabric preform at (…) °C	Alumina foam at (…) /°C	Quartz at (…) /°C
25	25	25	25
300	300	25	25
600	600	100	25
900	900	200	25
1200	1200	300	25

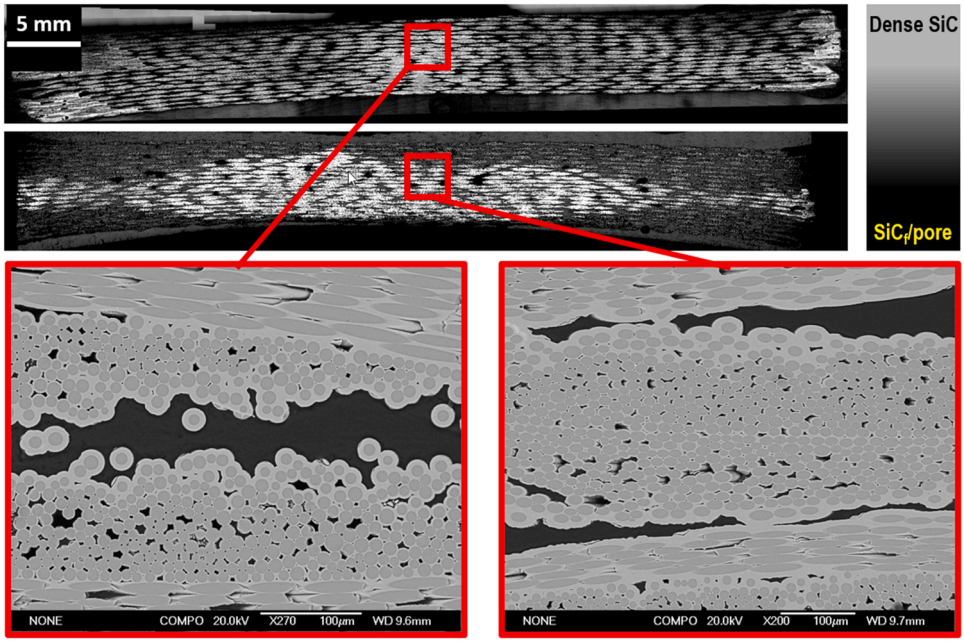

Fig. 8. Two optical microscope images showing inverse densification profiles of two SiC_f/SiC composites after 8 h of infiltration. Two micrographs at the bottom are magnified images of the centres of the composite and show nearly 5 μm of SiC deposit encasing the fibres.

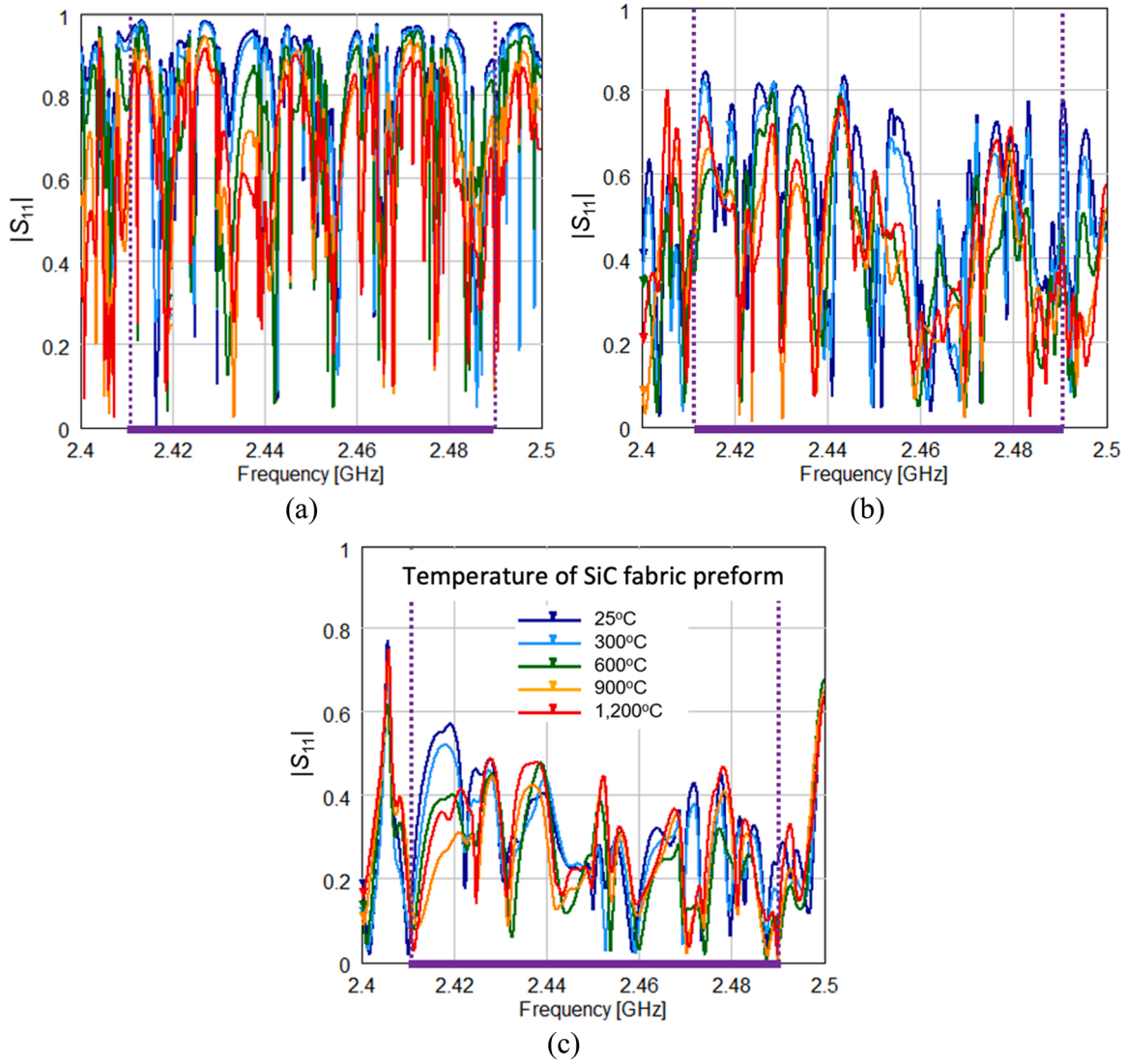

Fig. 9. Simulated frequency characteristics of magnitude of the reflection coefficient in the microwave system for different sizes of the SiC fabric: preform *A* (a), preform *B* (b), and preform *C* (c) and for five temperatures of the SiC fabric. A colour version is available at https://doi.org/10.1016/j.jeurceramsoc.2022.12.035

3.2. Materials parameters of ME CVI components

Whilst accurate reproduction of the experimental system and precision of the applied numerical method are important to develop a representative simulation, reliable data on material parameters is fundamental to success. Adequate simulation of microwave heating in the ME CVI process requires the use of both EM and thermal parameters for each component of the experimental set up (i.e., the SiC fabric preform, Al_2O_3 foam and quartz) as functions of temperature over the entire temperature range (20–1200 ℃). To this end, data on ε', ε'', ρ, C_p, and k all needed to be known. For the SiC fabric sample, all data were collected experimentally, whereas that for the alumina foam and quartz were taken from literature and appropriately adjusted with the use of suitable mixture models. The following sub-sections detail how this data was collected.

3.2.1. Dielectric properties

Dielectric property measurements were carried out by the Microwave Division, ITACA, Universitat Politecnica de Valencia, Spain. Complex permittivity at room and elevated temperatures were measured in an inert atmosphere to prevent oxidation [36]. Samples of the.

Hi Nicalon Type-S SiC fibre were prepared by first removing the sizing and then a combination of cutting, milling and grinding used to turn the fabric into a powder with a $D_{50} = 3$ μm. The powder was as densely packed as possible into a quartz tube, with a volume measuring 9×15 mm, to reduce the impact of porosity on the measurement. The electromagnetic properties of the foam structures were adjusted accordingly using a weighted mean calculation, the electromagnetic properties of air and the theoretical density of solid alumina [37]. The complex permittivity of quartz was taken from [31].

Fig. 6 shows the dielectric constant and the loss factor of all three materials as functions of temperature. Both ε' and ε'' of the SiC fibre steadily increased with temperature, reaching maximum values near 20. At elevated temperatures, dielectric constant showed a more linear behaviour above about 400 °C, whereas the loss factor exhibited a more exponential curvature, which is suggestive of thermal runaway at higher temperatures. Strong nonlinearity of temperature-dependent complex permittivity also indicates that in the EM-thermal iterative procedure the HTS should be sufficiently small to ensure adequate simulation of time evolution of the temperature field. For the quartz, the complex permittivity was almost constant with temperature, with ε' increasing from room temperature to 1200 ℃ by only 0.01 and being very close to zero for ε''. The alumina foam also had a very low ε'', whilst the ε' value

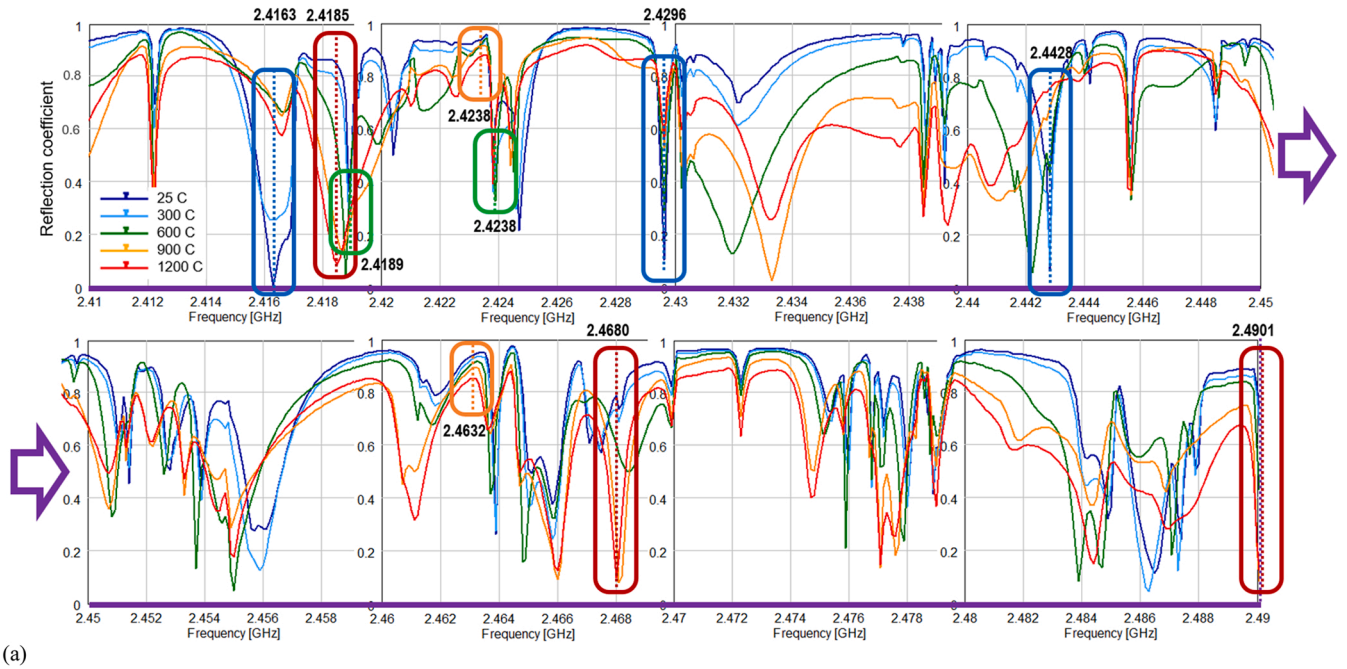

(a)

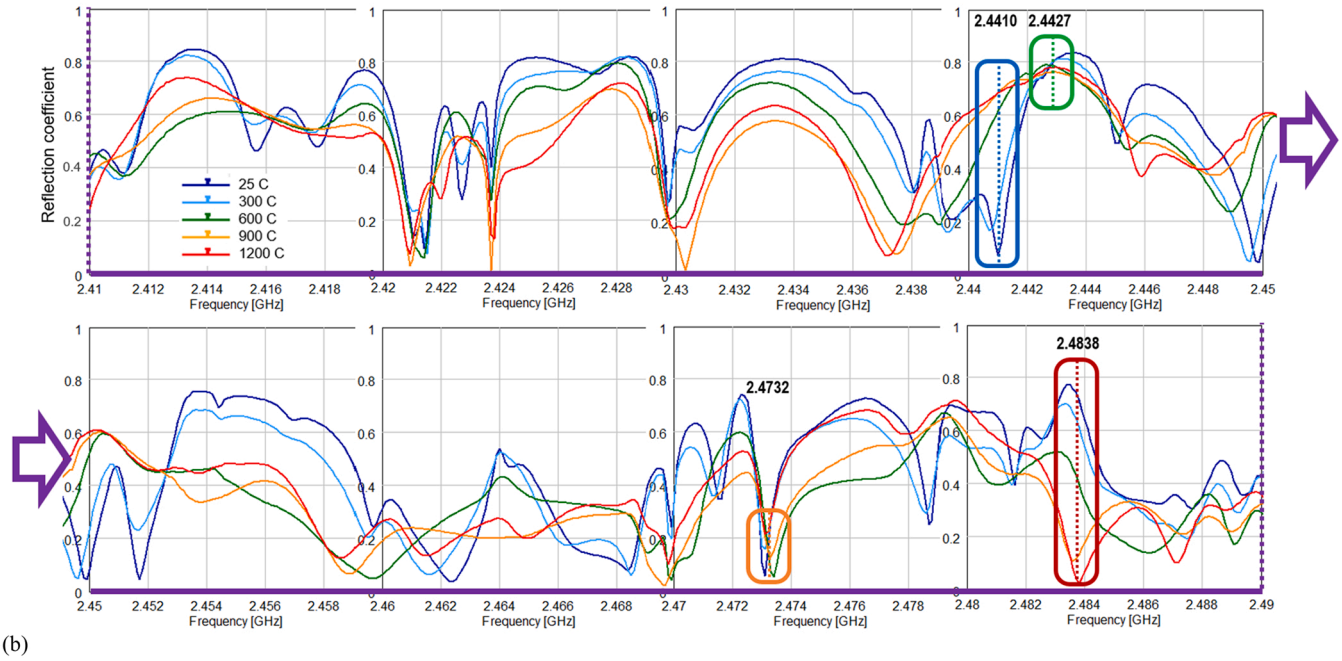

(b)

Fig. 10. Exploded views of the three figures in Fig. 9 for preforms *A* (a), *B* (b) and *C* (c). Blue, red, green and orange frames highlight chosen frequencies providing decreasing, increasing, constant high and constant low energy coupling, respectively (see Table 4).

increased steadily above ~200 °C.

3.2.2. Thermal parameters

The values of density that were adopted in the model are shown in Table 1. The theoretical density of the SiC fibre was 3.1 g cm^{-3} [38]; as the preform was a porous material, the density was calculated based on the volume fractions of fibres (~20%) and air (~80%), meaning the preforms used in the experimental work had a density of 0.48 g cm^{-3}. The density for bulk.

Al_2O_3 is 3.97 g cm^{-3} [39] and the bulk density of the foams was calculated to be 0.49 g cm^{-3}. The quartz density was 2.2 g cm^{-3}. The drop in density due to thermal expansion was estimated for all materials to be about 0.001 g cm^{-3} and was ignored in the model.

Measurements of specific heat and thermal diffusivity as a function of temperature were carried out using the ASTM E1269 and ASTM E1461, respectively [19,20,40]. The resulting temperature characteristics of all the materials are shown in Fig. 7(a). At elevated temperatures, C_p values of the alumina foam and quartz both turned out to be higher than that of the SiC fibre by 0.2–0.3 J g °C^{-1}.

The interpolated data for specific heat capacity and thermal diffusivity was then used to calculate the thermal conductivity k:

$$k = \alpha C_p \rho \quad (1)$$

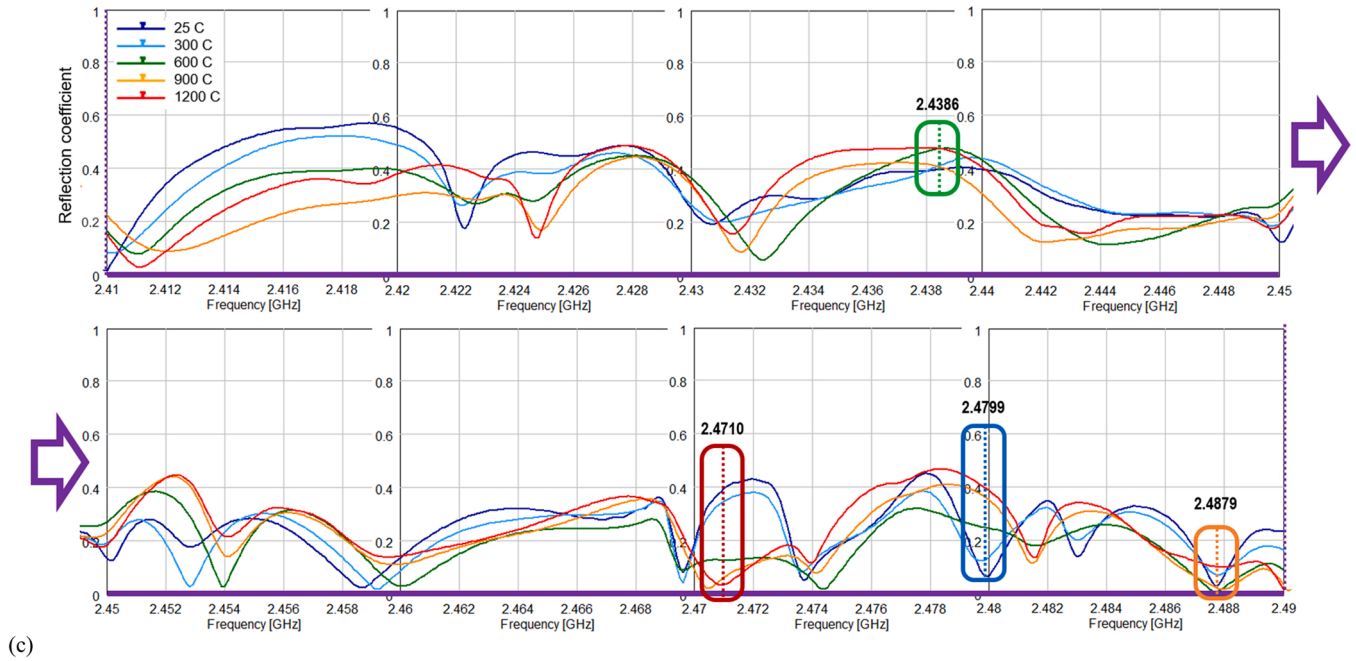

(c)

Fig. 10. (*continued*).

Table 4
Four heating scenarios based on temperature / time variation of $|S_{11}|$ at a fixed frequency that was used to compare the heating rates and time evolutions of different temperature fields.

Condition	Frequencies selected (GHz)		
	A $d = 55$ mm, $h = 8$ mm	*B* $d = 110$ mm, $h = 16$ mm	*C* $d = 165$ mm, $h = 24$ mm
Increasing $\|S_{11}\|$, Energy coupling decreasing with temperature (Yellow)	I: 2.4163 II:2.4428 III: 2.4296	I: 2.4410	I: 2.4799
Decreasing $\|S_{11}\|$, Energy coupling increasing with temperature (Green)	IV: 2.4185 V: 2.4680 VI: 2.4901	II: 2.4838	II: 2.4710
Constant low $\|S_{11}\|$, Energy coupling constantly high (Cyan)	VII: 2.4189 VIII: 2.4238	III: 2.4732	III: 2.4879
Constant high $\|S_{11}\|$, Energy coupling constantly low (Grey)	IX: 2.4632 X: 2.4480	IV: 2.4427	IV: 2.4386

where α is thermal diffusivity. It is worth noting that this parameter is an inherent material property, therefore the theoretical density for all the materials was used in the calculations rather than the effect of the bulk density, which is accounted for in the simulation calculations as it is a separate parameter. At temperatures below 400 °C, the alumina foam's thermal conductivity was higher than that of the SiC fibre preform due to the higher theoretical density of Al_2O_3 whilst k of quartz remained relatively constant at a mean of 0.015 W cm ℃$^{-1}$, Fig. 7(b).

4. Results and discussions

In this study, the EM and coupled EM-thermal simulations were conducted on a Dell workstation (64-bit Windows 10) with two Intel Xeon gold 5120 processors with a peak frequency of 3.2 GHz. The processors had 14 cores and supported 28 threads. The workstation also employed the GPU NVIDIA Quadro P500.

To optimise the size of the model (and keep the CPU time practical), non-uniform meshes with adjusted cell sizes, depending on the wavelength in the media, were applied to discretise the solution space within the cavity; that way a high degree of accuracy of the simulation was ensured. Parameters of the mesh for different sizes of the SiC samples and different materials along with the size of the model are given in Table 2.

In the EM modelling, simulation of one scenario that reaches steady state solution took, depending on the size of the SiC fabric preform and the values of complex permittivity, from 0.5 to 2 h. When solving the coupled problem, the HTS was set from 0.5 to 5 s, depending on the heating rate of the sample; as such, the simulation of the entire heating process took about 5 h of CPU time for the shortest scenario and about 75 h for the longest.

4.1. Experiments in processing of SiC_f/SiC composites

The practical experiments successfully demonstrated the efficiency of the ME CVI process for production of SiC_f/SiC composites [19,20]. Two samples partially densified successfully via the ME CVI of two SiC_f preforms are shown in Fig. 8; the brighter areas are the evidence of substantial amounts of deposited SiC deposited. Calculations based on the experiments show the clear potential for achieving full density in approximately 100 h; this would translate into more than an order of magnitude time reduction compared with conventional CVI production of an equivalent CMC.[3]

It must be stressed, however, that the samples shown in Fig. 8 were in the minority – only approximately 20% of produced samples showed this desired densification profile. The majority of samples showed a homogenous deposition profile, with some also showing regions of increased deposition due to hot spot occurrence. In all the experiments, it was practically impossible to predict how identical samples would behave in the microwave field. For instance, there were significant heating rate changes during microwave processing whilst the input

[3] Note that since it is only possible to undertake CVI using methyltrichlorosilane (with an off-gas of hydrogen chloride) for 8 h per day due to Health & Safety at UoB, even 100 h means that it would take approximately 12 days to make each sample in the laboratory.

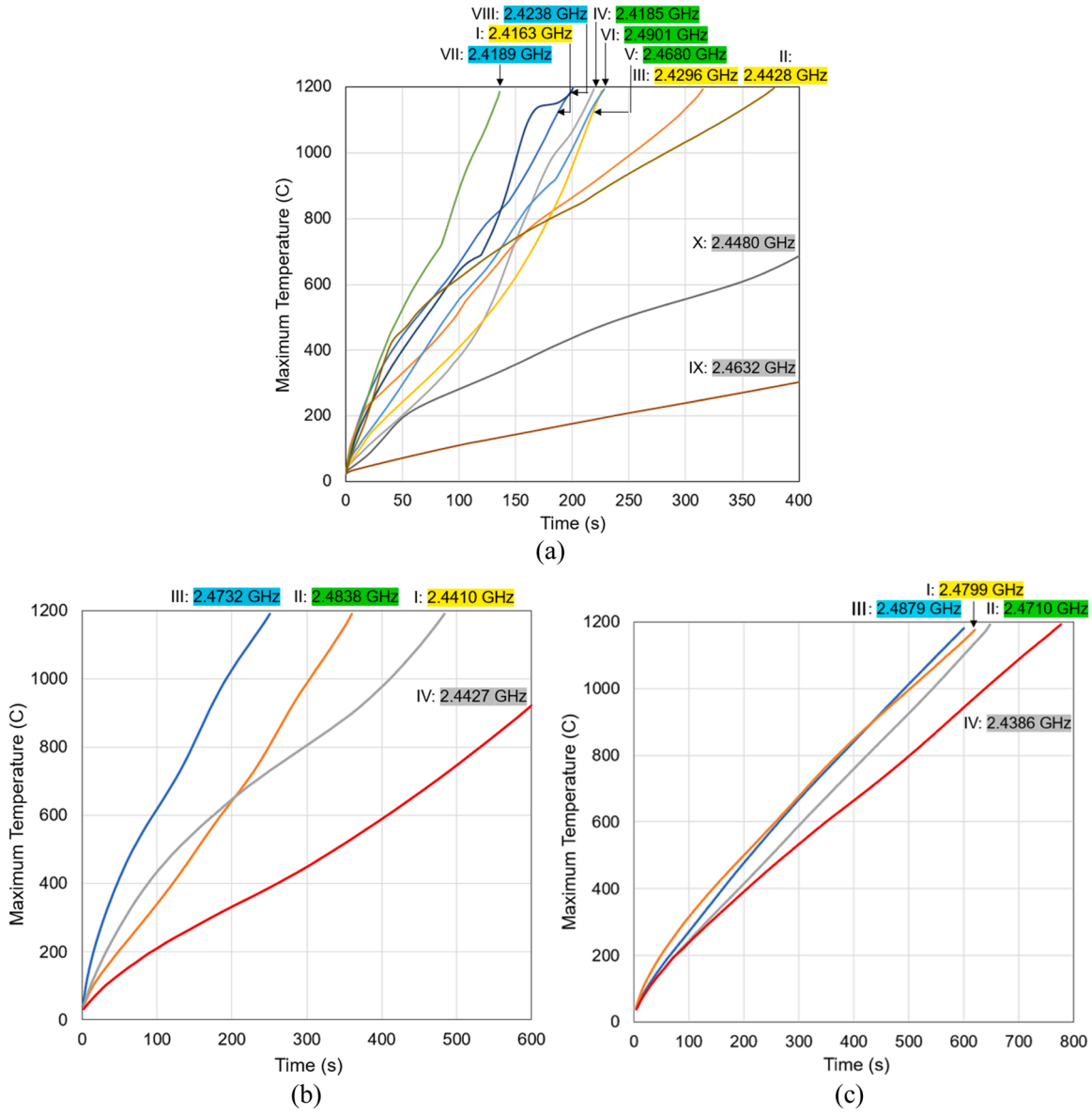

Fig. 11. Time characteristics of maximum temperature in the SiC fabric sample – preforms A (a), B (b), and C (c) – at different frequencies providing decreasing, increasing, constant high and constant low energy coupling, as specified in Table 4; input power 1.1 kW.

power remained constant, and some (supposedly identical) samples coupled with the field much better than others.

These results ultimately prompted the demand to develop a suitable computer model capable of providing insight into the interaction of microwaves with the processed samples, clarification of the reasons for the unexplained experimental phenomena, and understanding of the factors behind the lack of the reproducibility of the process.

4.2. Computational results

4.2.1. Reflection coefficient (energy coupling)

The issue of unpredictable heating rates in the experimental production of the SiC_f/SiC composite before densification was addressed through the analysis of energy efficiency of the microwave processing system. In the realm of electromagnetic modelling, energy efficiency can be conveniently evaluated with the help of the frequency characteristics of the magnitude of the reflection coefficient $|S_{11}|(f)$ that are determined at the cross-section of the feeding waveguide [30]. In particular, low values of $|S_{11}|$ in a wide frequency range suggest that, regardless of the fluctuation of the frequency spectrum in the magnetron source of microwave power, energy coupling stays nearly constant, changes of the microwave heating rate are negligible and performance of the system remains stable [41–43].

The goal was to analyse the change of the $|S_{11}|(f)$ characteristics during microwave processing, i.e., for different temperatures of the materials. Since computation of S-parameters is power-independent, temperature was introduced as a parameter in these simulations via corresponding values of $\varepsilon'(T)$ and $\varepsilon''(T)$. Preliminary multiphysics modelling allowed estimation that when, during the heating process, the average temperature of the SiC fabric sample reached its maximum (1200 °C), the average temperature of the adjacent alumina holders had increased to approximately 300 °C and the heating of the quartz elements was nearly negligible. Table 3 specifies how the values of permittivity, and the loss factor were defined in the model to enable simulation of $|S_{11}|(f)$ for five values of T in the temperature range from 25 to 1200 °C. It is worth noting that in the subsequent systematic simulation of temperature fields in different heating scenarios we later saw alumina ring heated up to higher temperatures. However, since the

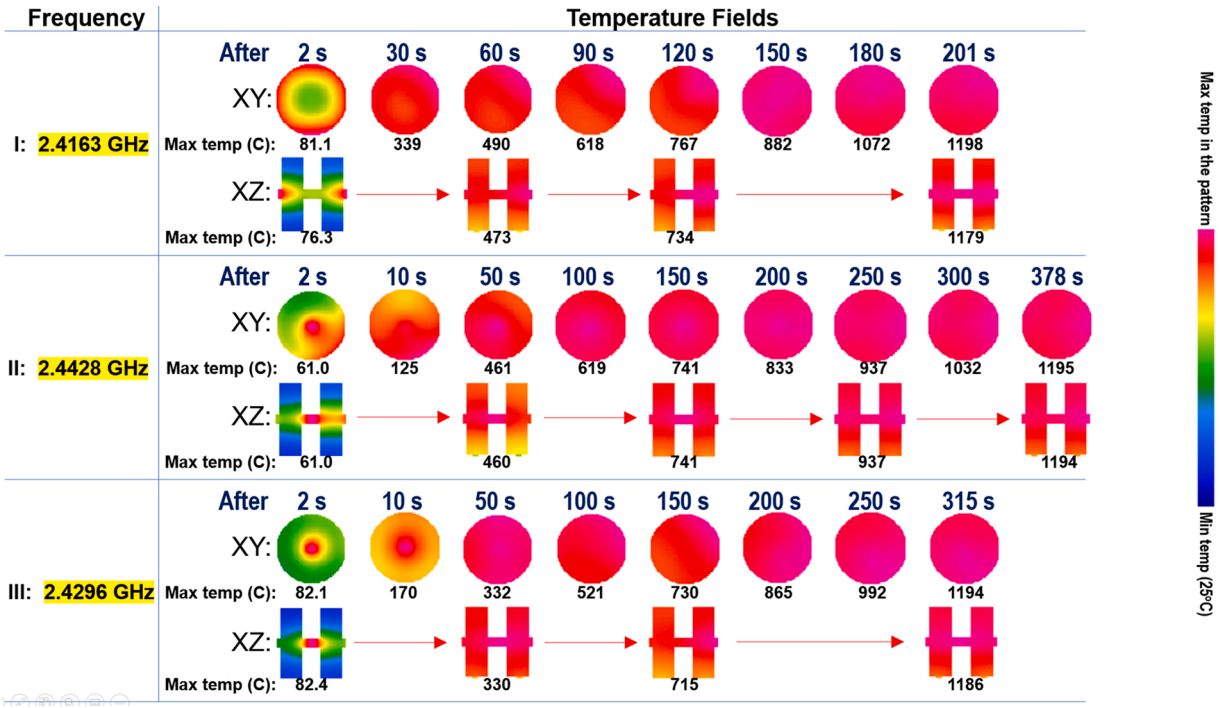

Fig. 12. XY-and XZ-cross sectional temperature profiles of the heating processes in preform *A* in accordance with scenario (1) at three frequencies (I to III), as seen in Table 4. Corresponding time instances and values of maximum temperatures are above and below the patterns.

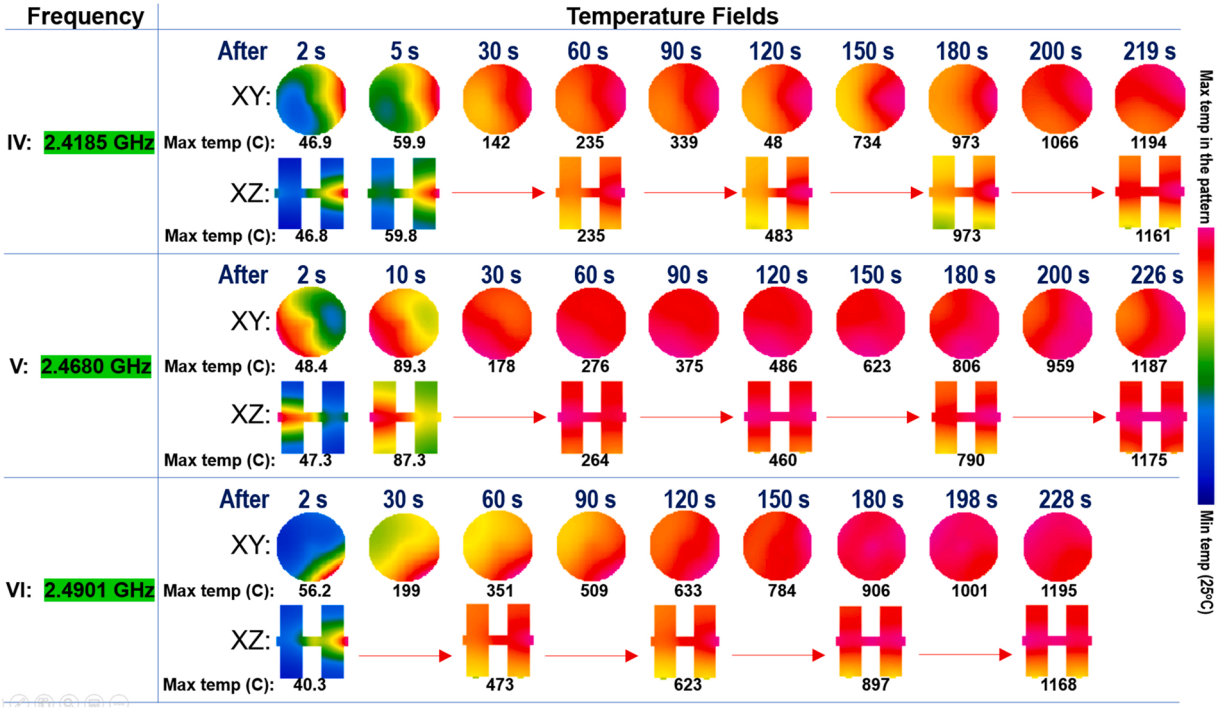

Fig. 13. XY-and XZ-cross sectional temperature profiles of the heating processes in preform *A* in accordance with scenario (2) at three frequencies (IV to VI), as seen in Table 4. Corresponding time instances and values of maximum temperatures are above and below the patterns.

EM process in this system is mostly conditioned by much higher values of complex permittivity of SiC fabric preform, we believe that the choice of dielectric constant and the loss factor for alumina foam on the levels below.

300 °C may not notably change the main trends in the revealed behaviour of the of $|S_{11}|(f)$ curves. Energy efficiency C at each frequency was then estimated from the formula:

$$C\ (\%) = (1 - |S_{11}|^2)100\% \tag{2}$$

Fig. 9 shows the graphs of the simulated frequency characteristics of the reflection coefficient for the SiC fabric preforms of three different sizes. The data shows that samples with the smallest volume (*A*) have the

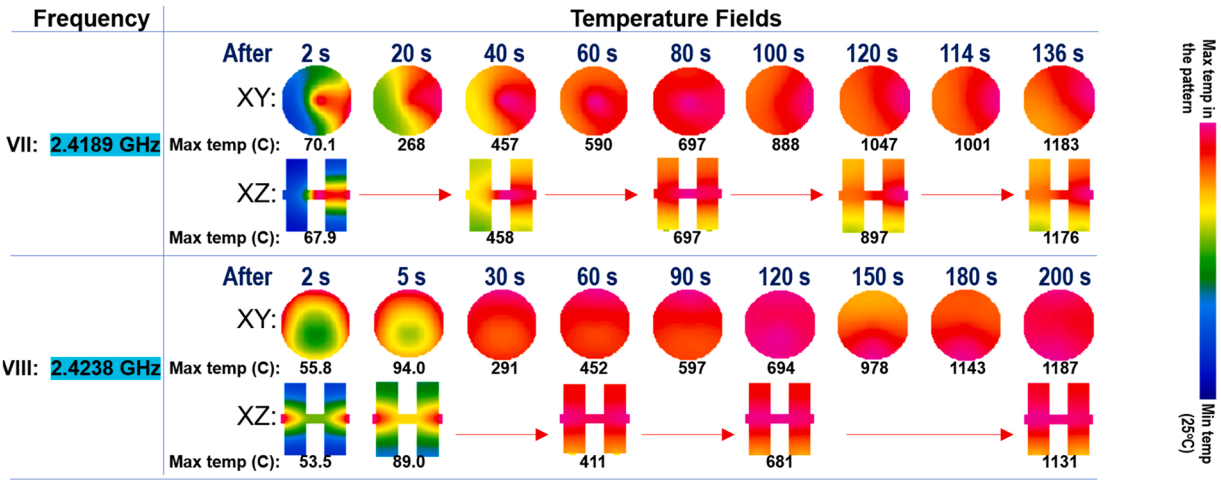

Fig. 14. XY-and XZ-cross sectional temperature profiles of the heating processes in preform *A* in accordance with scenario (3) at three frequencies (VII & VIII), as seen in Table 4. Corresponding time instances and values of maximum temperatures are above and below the patterns.

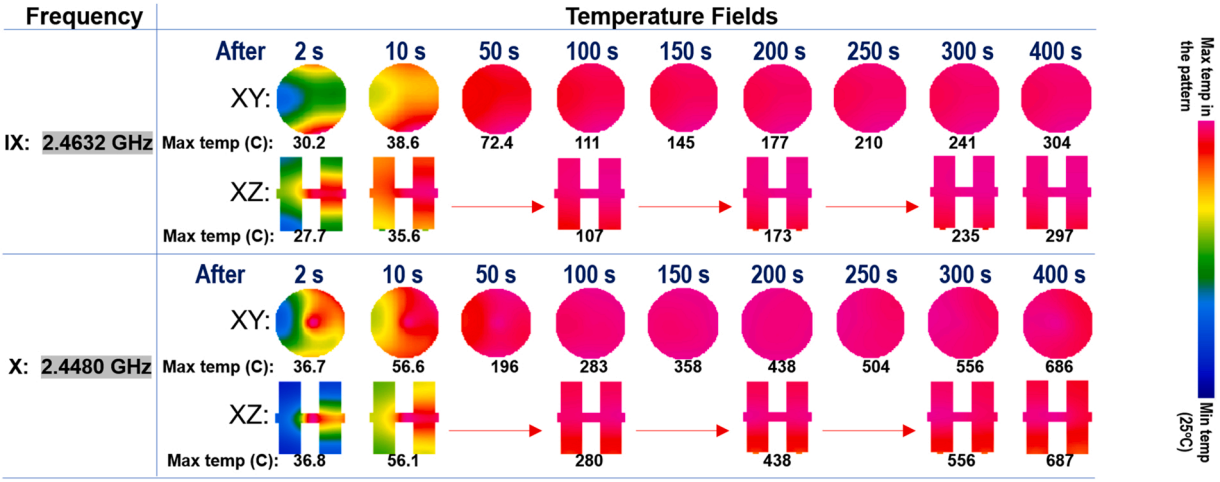

Fig. 15. XY-and XZ-cross sectional temperature profiles of the heating processes in preform *A* in accordance with scenario (4) at three frequencies (IX to X), as seen in Table 4. Corresponding time instances and values of maximum temperatures are above and below the patterns.

highest reflection coefficient with a mean value of 0.51, whilst the largest samples (*C*) had the lowest $|S_{11}|$, a mean value of 0.23. This is consistent with the fact that larger SiC samples have the highest absorption [44,45].

It can also be seen that the $|S_{11}|(f)$ curves are characterised by multiple narrow resonances. For such a big (compared to the wavelength) cavity of the microwave system and relatively small samples of the absorbing materials, this is natural as the system behaves as a resonator characterised by a high *Q*-factor.

From the detailed view of these curves visualised in Fig. 10 for the stretched frequency axis, one can, for example, observe that, for preform *A*, on the level of 0.3, the width of some resonances can be as small as 0.5 MHz, and, in the range from 2.43 to 2.47 GHz, there are as many as 12 such resonances. When matched against an irradiation spectrum of a typical magnetron, such characteristics serve as an indication of highly unstable performance by the microwave system. Hence, unpredictable and significant frequency variation of energy efficiency (and thus of the heating rates) might be a direct consequence for such a mismatch. The observed significant change of the reflection coefficient with frequency is consistent with the results in study [46] which, through a sensitivity analysis, concluded that frequency was the most critical factor in stability of the ME CVI process.

It can be also seen that, as the temperature of the SiC fabric preform increased, the profile of every $|S_{11}|$ curve changed. Variation in heating rates could, therefore, also result from the increase in temperature of the SiC preform; temperature, in its turn, depending on the duration of the heating process.

In the next sub-sections, the focus is on how the temperature characteristics of the processed sample changed at specific frequencies with time.

4.2.2. *Time-temperature characteristics of the SiC preforms*

Since distributions of the electric field and dissipated power in the cavity and of temperature within the materials depend on frequency, the main goal for the coupled EM-thermal modelling was to analyse time evolutions of microwave-induced temperature fields at different frequencies of excitation prior to densification. Understanding the formation of temperature patterns and their advancement with time is a key to controlling equipment operation better and designing more efficient microwave-heating systems.

For a systematic analysis of the heating patterns, the time-wise behaviour of the reflection coefficient was characterised as belonging to one of the following four scenarios:

(1) $|S_{11}|$ was *low* at the beginning of the heating process, but strongly *increased* with increasing temperature.

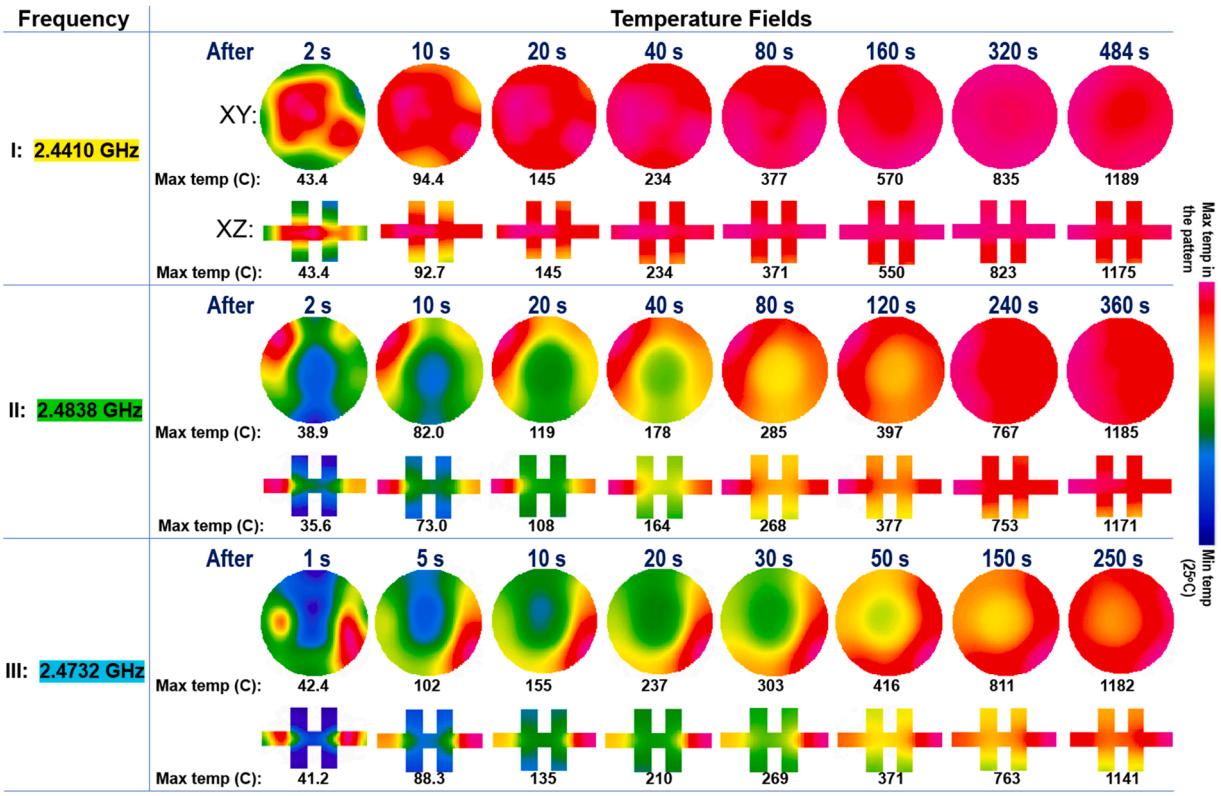

Fig. 16. A series of XY and XZ cross sectional time evolution of temperature profiles of the *B* preform SiC_f material during microwave heating at various frequencies corresponding to different scenarios as seen in Table 4.

(2) $|S_{11}|$ was *high* at the beginning of the heating process, but strongly *decreased* with increasing temperature.
(3) $|S_{11}|$ was *low* at the beginning of the heating process and *remained so* across the entire temperature range.
(4) $|S_{11}|$ was *high* at the beginning of the heating process and *remained so* across the entire temperature range.

To understand the graphs in Fig. 10 better, ten (I-X, preform *A*), four (I-IV, preform *B*) and four (I-IV, preform *C*) frequencies were identified that most eloquently represented the categories (1) to (4) above for the different SiC fabric preforms; these are gathered in Table 4.

The coupled EM-thermal simulation shows that the growth of the maximum temperature, T_{max}, of the SiC samples in different heating scenarios (1)-(4) may be significantly different. At those frequencies at which reflections stay low (and energy coupling is maintained high) in the course of the heating process (or, at least, in the beginning of it), the simulation suggests the heating rate is significantly higher than at the frequencies at which the reflection coefficient is high all the time.

For example, as seen from Fig. 11(a), for preform *A*, heating with input power 1.1 kW at frequencies IX and X (scenario (4)) for 400 s resulted in T_{max} being below 700 °C, whereas 1200 °C could be reached at frequencies I, VII, VIII for less than 200 s. These heating rates and their variability are consistent with those observed experimentally [19].

Modelling results also indicate that for the larger samples, preforms *B* and *C*, the dependence of the heating rate on frequency was less pronounced, Fig. 11(b), (c). This is explained by both the overall smaller values of $|S_{11}|$ and their lower variation with time / temperature. These samples took longer to reach 1200 °C despite the lower reflection coefficient. All curves show the same trend with the constantly low $|S_{11}|$ heating the fastest and the constantly high the slowest. It is worth noting that in reality more power, or a longer heating time would be needed for the larger discs to achieve the necessary temperatures, in particular when accounting for radiative losses that were not included in the model. Investigating this was outside the scope of this work, which aimed to highlight the importance of a corresponding simulation, however basic, is when using microwave energy to process ceramics.

The time-temperature characteristics in Fig. 11 are given for the maximum temperature in the sample at the given time instance. Heating at different frequencies resulted in distinct heat distributions and the location of the hottest spot was not necessarily the same throughout the heating process. The location may follow the time transformation of the pattern of the temperature field and either smoothly move or jump to different points in the heated sample, and the heating rates at those points might therefore be notably different. The latter effect explains the presence of the inflection points on some curves in Fig. 11(a).

It is also worth mentioning that, despite the increase of the loss factor of the SiC preforms with temperature, Fig. 6(b), thermal runaway did not emerge in any of the heating processes characterised in Fig. 11. This is also consistent with the experimental work.

4.2.3. *Temperature fields and their time evolution*

Visualisations of temperature fields were produced in the samples heated up to 1200 °C to compare pattern development of the Al_2O_3 foam - SiC fabric - Al_2O_3 foam sandwich in the central cross-sections in the XY- and XZ-coordinate planes. Figs. 12–15 show the evolutions of the relative temperature profiles in the microwave heating of the system with preform *A*, i.e., the pattern developments caused by frequencies I-X in all four heating scenarios (1)-(4), as shown in Table 4. Each pattern shows (using colours, from dark blue to magenta) temperature distribution between the minimum in the heating process (20 °C) and the.

maximum in the given pattern. Maximum temperature values are provided under each pattern; to estimate corresponding minimum value, one can refer to the colour bar on the right. In all cases illustrated in Figs. 12–15 input power was set up to be 1.1 kW.

Initial, i.e., after heating for 2 s, temperature distributions (closely reproducing patterns of dissipated power) at all frequencies appear, as

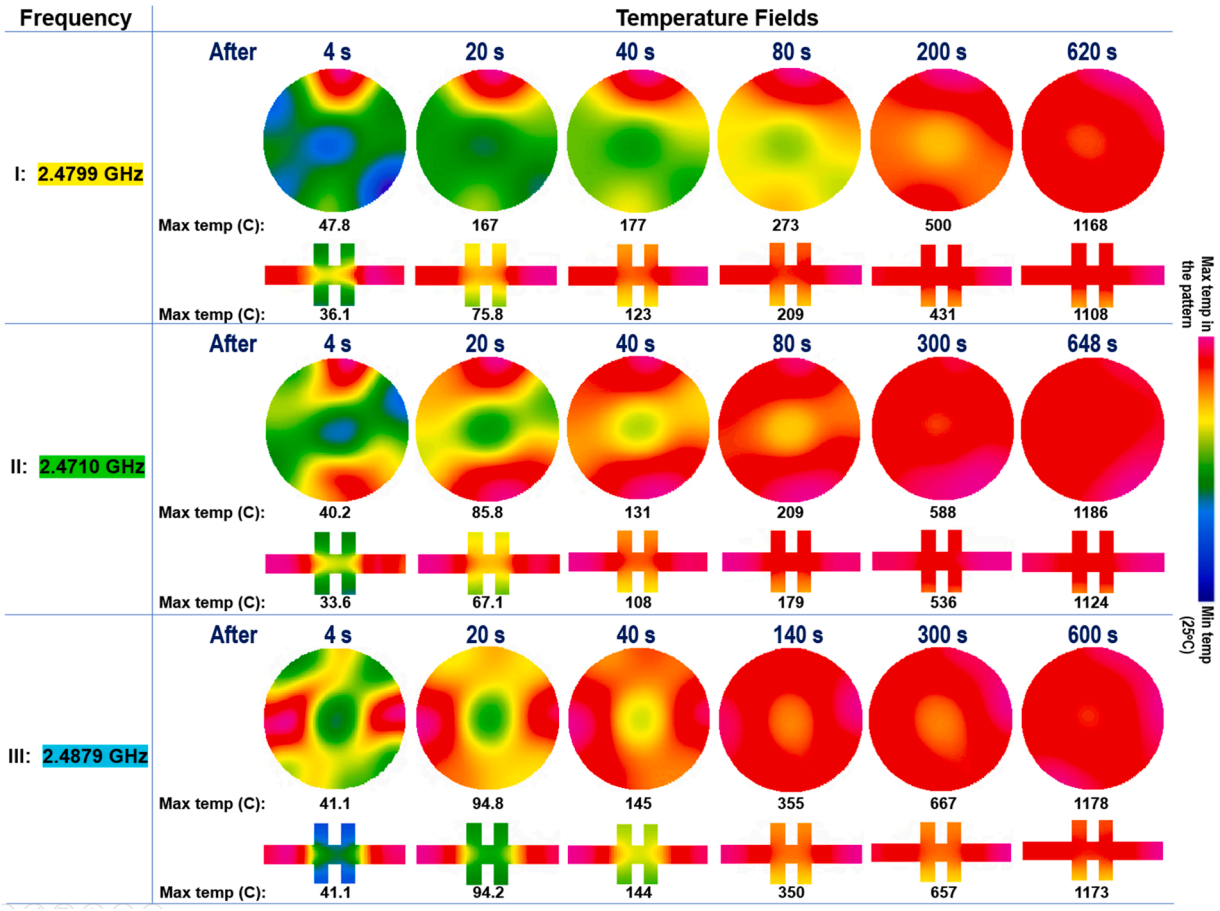

Fig. 17. A series of XY and XZ cross sectional time evolution of temperature profiles of the *C* fabric preform SiC_f material during microwave heating at various frequencies corresponding to different scenarios as seen in Table 4.

expected, to be very different. Maximum temperatures in these distributions strongly depended on the level of energy coupling. Their locations (*hot spots*) are either in the centre (frequency III), or on the edge (frequencies IV, VI), and their values vary from 82 °C (scenario (1), frequency III) to 28 °C (scenario (4), frequency IX). The patterns in Figs. 12–15 show in detail how the heat was spread with time within the heated materials. Due to the very distinct heating rates at different frequencies the top temperatures were reached over different times, however, it may be seen that within 30–60 s all the patterns became quite homogeneous across both planes, so, regardless of the heating rate, the SiC fabric sample was heated in all these processes relatively uniformly.

Analysis of the patterns suggests that the evolution of the temperature profiles may be a combination of two trends; amplification of dissipated power in the *hot spots* due to the high (and increasing with temperature) values of the loss factor of the SiC fabric and the spreading of the peaks of the temperature distributions due to the relatively high local thermal conductivity of the SiC fabric. Since maximum temperatures in the final simulated patterns.

differ by more than 500 °C, the process of homogenisation can be explained by a strong influence of thermal conductivity.

Another observation made from the heating patterns in Figs. 12–15 is the identification of the beneficial impact made by the Al_2O_3 foam rings on the temperature distribution in the system. It appears that the alumina holders also help dissipate *hot spots* formed in the SiC sample and effectively help to homogenise temperature within the processed material, again due to their relatively high local thermal conductivity. Having said this, it seems that the rings also provide some thermal insulation to the SiC fabric preform and thus slightly reduce the heat loss to the surrounding gaseous medium.

Thermal uniformity (whose benefits for CVI were particularly highlighted in the literature, see, e.g., [14,44]) was commonly observed in the ME CVI densification process described in Section 4.1. The simulation results that illuminate the process of temperature homogenisation discussed here are consistent with the experimental results.

Time evolutions of the temperature fields in the larger samples (preforms *B* and *C*) that take place at three frequencies corresponding to scenarios (1) to (3) are presented in Figs. 16 and 17. Similar to the smaller preform *A*, in the beginning of the heating process the temperature distributions induced by the microwaves at different frequencies are dramatically different. However, because of the larger diameters, the time required to homogenise the temperature distributions now clearly depends on the level of uniformity in the initial pattern. For example, a wide-spread hot spot in preform *B* (frequency I) may be homogenised in about 10 s, whereas, when starting from small strong peaks (frequencies II and III), the patterns become relatively uniform only after 200–250 s when the temperature of the sample has already reached 800–1200 °C. A similar trend is observed with preform *C*. In all cases, the time to get to the top temperatures of the process (1200 °C) is now longer; 250–650 s. Note.

that compared to the duration of a typical ME CVI densification run, estimated to be ~100 h to achieve 'full' densification [19,20] these times to achieve homogenisation of the heating are insignificant.

These results further highlight the significance of the locally high thermal conductivity of SiC fabric that it is believed makes it possible to eventually obtain the required level of heating uniformity (potentially for samples with diameters up to at least 200 mm), despite the intrinsically non-uniform heating by microwaves. This, in turn, makes the ME

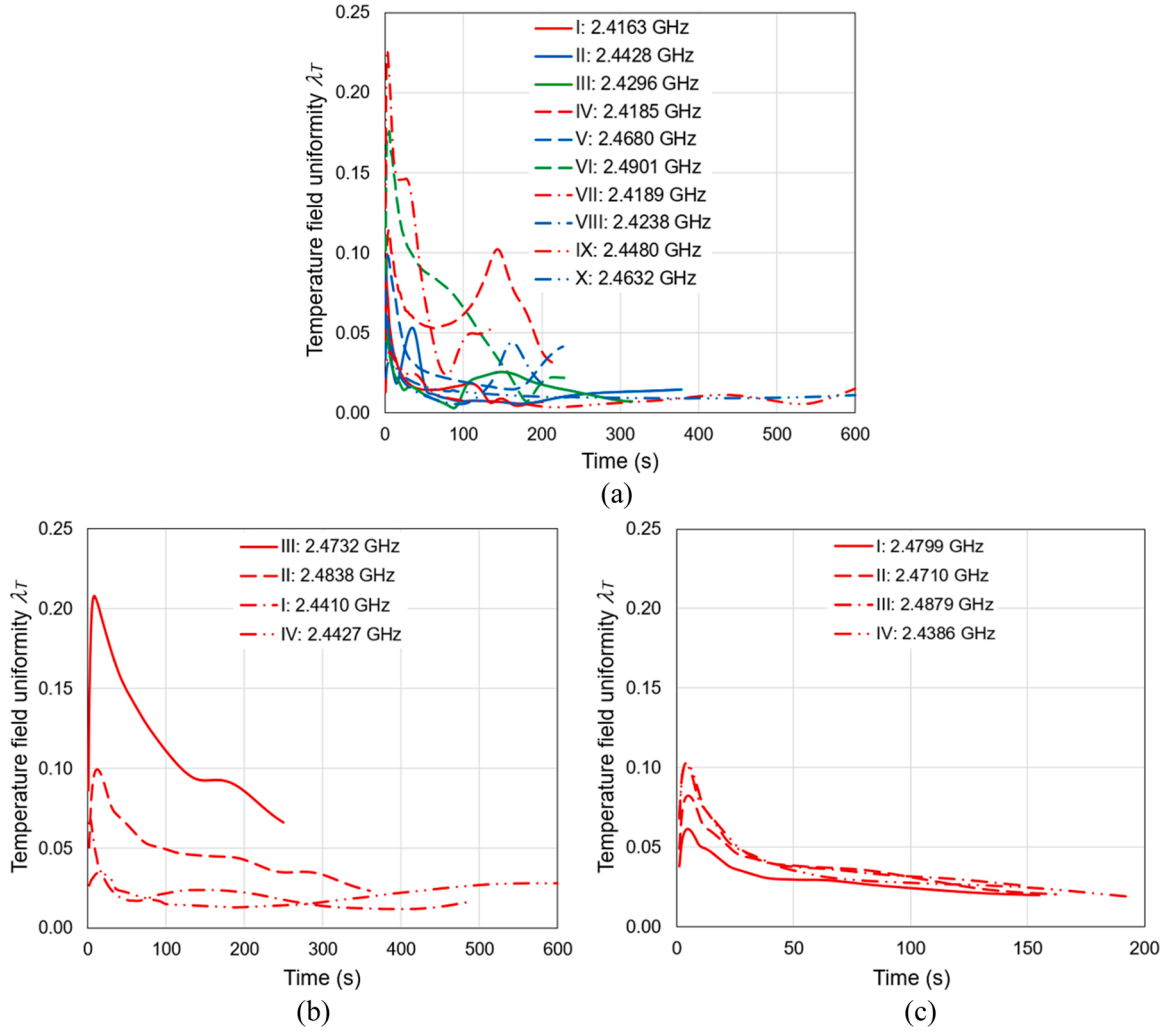

Fig. 18. Time evolution of the metric of the uniformity of the temperature fields, λ_T, induced by the microwaves in (a) preform *A* (frequencies I-X), (b) preform *B* (frequencies I-IV) and (c) preform *C* (frequencies I-IV).

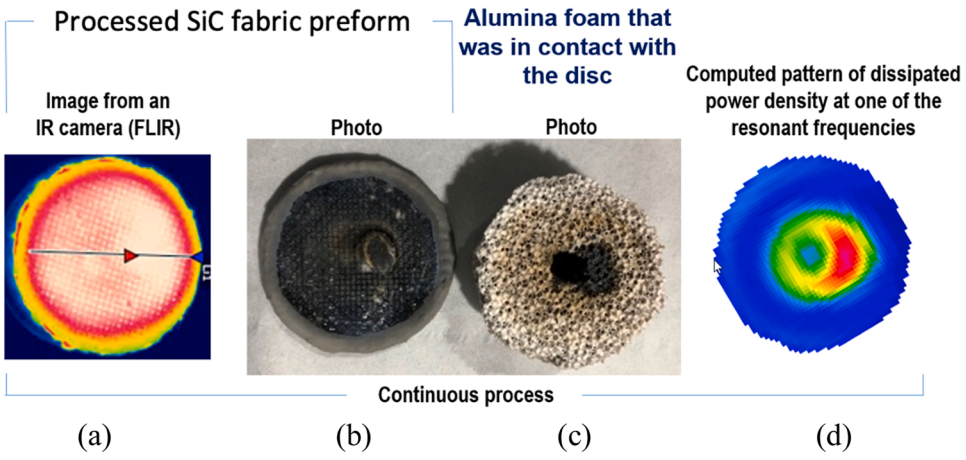

Fig. 19. An image of a SiC preform heated without one of adjacent Al_2O_3 foam rings to allow an infra-red image to be taken in-situ heated to 750 °C; (a) a hot spot off centre is marked by the red arrow; (b) a photo of the same sample with the Al_2O_3 foam ring put on the top of the sample after 8 h of infiltration; (c) the resulting cross section of the composite – the off-centre area with increased density appears blackened; (d) the simulated pattern of dissipated power; the hot spot appears in the off-centre area.

CVI process attractive for the processing of SiC_f/SiC composites. It also appears that the process of temperature homogenisation takes longer for preform *B* and *C* because of the weaker effect produced, in terms thermal insulation, by the alumina rings, which were only considered to be of the same size as preform *A*.

To achieve a more detailed understanding of the formation of the microwave-induced temperature fields prior to densification, the simulated patterns for all three preforms *A*, *B* and *C*, Figs. 12–17, were analysed with the use of a computational procedure [47] that quantitatively evaluated the level of uniformity of the temperature field, λ_T [48]. The corresponding metric was based on the ratio of the standard deviations and the means of the temperature values in the cells of the

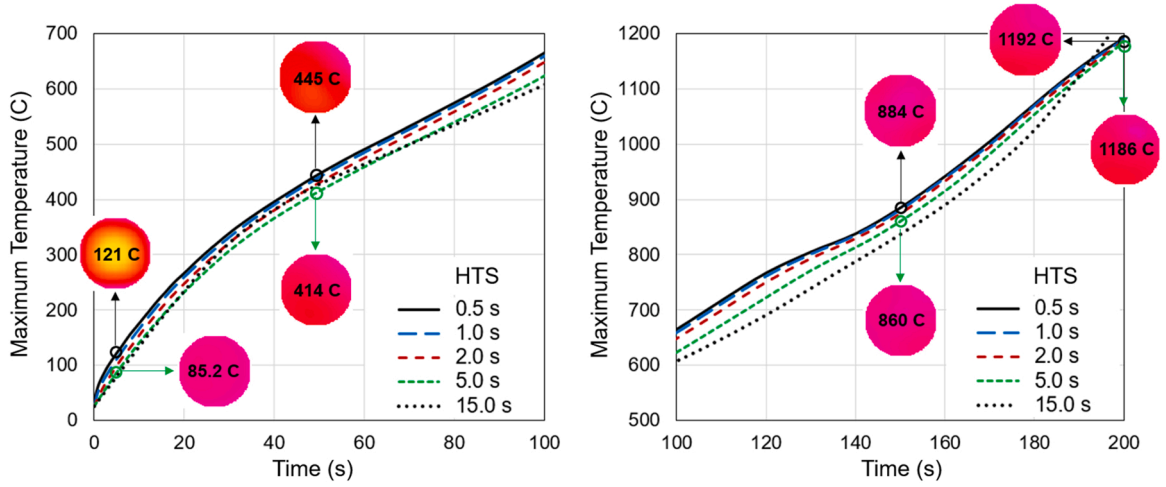

Fig. 20. Time characteristics of maximum temperature development in the SiC fabric sample (disks *A*) for decreasing coupling (scenario (1)) at frequency I for different HTS (from 0.5 to 15 s); corresponding temperature patterns in the central XY-plane through the disk (along with the values of T_{max} in those patterns) are shown for the time instances of 5, 50, 150 and 200 s for HTS = 0.5 and 5 s; patterns are normalised, similarly to Figs. 12–17, to minimum temperature of the process and maximum temperature in the pattern; input power 1.1 kW.

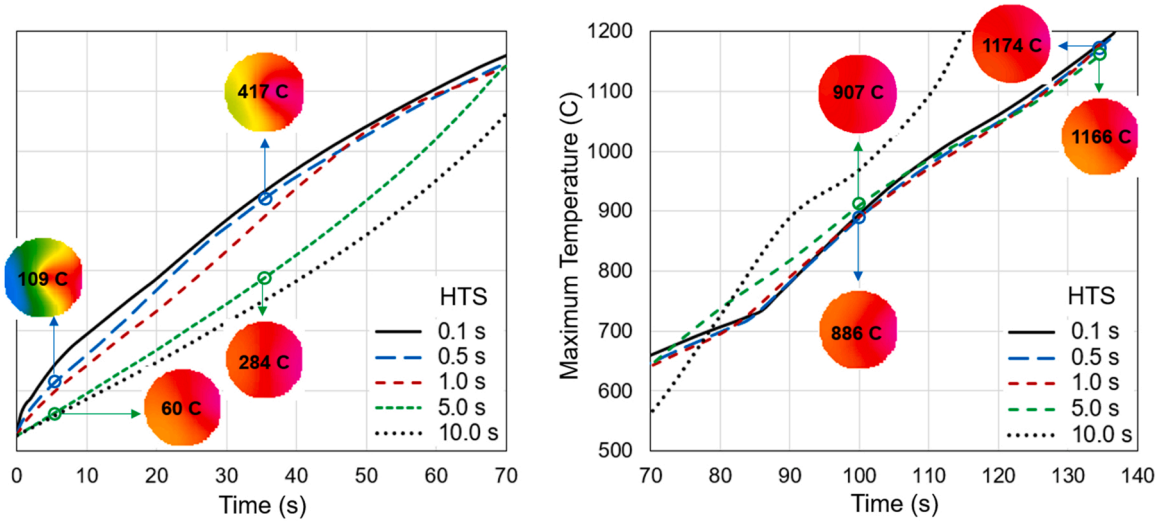

Fig. 21. Time characteristics of maximum temperature development in the SiC fabric sample (disks *A*) for constantly high coupling (scenario (3)) at frequency VII for different HTS (from 0.5 to 8 s); corresponding temperature patterns in the central XY-plane through the disk (along with the values of T_{max} in those patterns) are shown for the time instances of 5, 50, 35, 100, and 135 s for HTS = 0.5 and 5 s; patterns are normalised, similarly to Figs. 12–17, to minimum temperature of the process and maximum temperature in the pattern; input power 1.1 kW.

FDTD discretisation after every heating time step. As such, the more uniform the distribution, the smaller the value of λ_T.

This metric is plotted in Fig. 18 against the heating time for the SiC fabric preform *A*, *B* and *C*; the patterns reflecting the faster and slower microwave heating processes are quantitatively depicted there by the time characterisation of λ_T. The generally decreasing values of the uniformity metric confirm what can be visually observed in Figs. 12–17, the homogenisation of the temperature patterns occurs with increased heating time and hence temperature. It is also seen that whilst the slower heating processes in the SiC samples considered were caused by weaker energy coupling, they lead to more homogeneous temperature distributions.

5. Discussion and conclusions

The present paper has demonstrated the feasibility of producing SiC_f/SiC composites by ME CVI in which the SiC fibre preforms were heated in a SAIREM Labotron HTE M30KB CL PRO microwave system. Whilst the practical experiments showed clear potential for achieving full density of the composites in a significantly shorter time than in the conventional CVI production [19,20] the focus of this paper was to present corresponding modelling results obtained with the goals of:

- better understanding the macroscopic mechanisms of interaction between the microwaves and the SiC fabric preforms;
- clarify the causes for some experimental issues; and
- illustrate the potential to further develop the ME CVI process.

To this end, with the use of the FDTD EM model of the experimental scenario, it has been demonstrated that, when microwave processing a small SiC sample, energy coupling, as the 'derivative' of the reflection coefficient, is extremely sensitive to frequency. For example, a jump in the $|S_{11}|$ value from 0.05 to 0.75 may be caused by as small drift as 0.003–0.005 GHz. The frequency dependency is consistent with an observation derived from the relevant computational studies of microwave thermal processing of small ceramic samples in large cavities, e.g.,

Table 5
Electromagnetic and thermal material parameters of SiC fabric – numerical values used in the model.

Temp. (°C)	eps'	eps"	Cp (J/gC)	k (W/cmC)
25	5.44	1.059	0.631	0.007
100	5.47	1.153	0.785	0.008
200	5.62	1.327	0.900	0.008
300	6.02	1.577	0.950	0.008
400	6.78	1.937	0.974	0.007
500	7.93	2.456	0.987	0.007
600	9.49	3.203	0.996	0.007
700	11.4	4.278	1.001	0.006
800	13.5	5.826	1.005	0.006
900	15.8	8.055	1.008	0.006
925	16.3	8.751	1.008	0.006
950	16.9	9.514	1.009	0.006
975	17.5	10.349	1.009	0.006
1000	18.0	11.264	1.010	0.006
1025	18.6	12.266	1.010	0.006
1050	19.1	13.363	1.011	0.006
1075	19.6	14.565	1.011	0.006
1100	20.1	15.882	1.011	0.006
1125	20.6	17.324	1.012	0.006
1150	21.1	18.904	1.012	0.006
1175	21.6	20.635	1.012	0.006
1200	22.1	22.530	1.013	0.006

Table 6
Electromagnetic and thermal material parameters of alumina foam – numerical values used in the model.

Temp. (°C)	eps'	eps"	Cp (J/gC)	k (W/cmC)
25	1.97	0.024	0.756	0.040
100	2.14	0.025	0.898	0.032
200	2.38	0.029	1.022	0.025
300	2.64	0.036	1.102	0.019
400	2.93	0.049	1.155	0.016
500	3.25	0.071	1.191	0.013
600	3.62	0.100	1.216	0.011
700	4.04	0.139	1.235	0.010
800	4.54	0.189	1.250	0.009
900	5.13	0.251	1.261	0.008
925	5.29	0.269	1.263	0.008
950	5.46	0.287	1.265	0.008
975	5.64	0.306	1.267	0.008
1000	5.83	0.326	1.269	0.008
1025	6.02	0.347	1.271	0.007
1050	6.23	0.369	1.273	0.007
1075	6.44	0.392	1.274	0.007
1100	6.67	0.415	1.276	0.007
1125	6.90	0.439	1.278	0.007
1150	7.15	0.465	1.279	0.007
1175	7.42	0.491	1.280	0.007
1200	7.69	0.518	1.282	0.007

the frequency-domain simulation of ME CVI [46] and the time-domain modelling of microwave heating of zirconia [31].

On the other hand, because of the temperature dependency of the complex permittivity of the SiC fabric and Al_2O_3 foam involved in the process, the coupling also changes during the course of heating, even when the frequency is fixed. Therefore, during the microwave processing excited by the Labotron's magnetron generator, the heating rate may indeed be unpredictable; it may either stay high, or low, or vary significantly.

It has also been shown that the time required to reach the maximum temperature of the process, 1200 °C, in the SiC fabric preform was strongly depends on both the size of the sample and the degree of energy coupling. For example, with 1.1 kW of input power, when the heating rate was constantly high, the time to achieve the maximum temperature in the stacked discs with diameters from 55 to 165 mm ranged from 130 to 600 s, respectively, whereas, with a low heating rate in the 55 mm sample, over same amount of time, the sample reached < 200 °C.

Table 7
Electromagnetic and thermal material parameters of quartz – numerical values used in the model.

Temp. (°C)	eps'	eps" ($\cdot 10^{-4}$)	Cp (J/gC)	k (W/cmC)
25	3.84	2.35	0.602	0.014
100	3.85	2.35	0.856	0.015
200	3.85	2.35	0.976	0.016
300	3.86	2.35	1.040	0.017
400	3.88	2.42	1.081	0.018
500	3.89	2.42	1.111	0.018
600	3.89	2.42	1.134	0.018
700	3.90	2.42	1.153	0.018
800	3.91	2.50	1.168	0.017
900	3.92	2.50	1.180	0.016
925	3.92	2.50	1.183	0.015
950	3.93	2.50	1.186	0.015
975	3.93	2.57	1.189	0.015
1000	3.93	2.57	1.191	0.014
1025	3.93	2.57	1.194	0.014
1050	3.94	2.57	1.196	0.013
1075	3.94	2.57	1.199	0.013
1100	3.94	2.57	1.201	0.013
1125	3.94	2.64	1.203	0.013
1150	3.95	2.6	1.205	0.012
1175	3.95	2.64	1.207	0.012
1200	3.95	2.64	1.209	0.012

The FDTD electromagnetic-thermal coupled model developed has revealed that microwave-induced temperature distributions are considerably different at different frequencies. The model has also helped interpret the formation and time evolution of the temperature fields in the experimental system. Simulation results have shown that the patterns, though initially non-uniform within the SiC sample, become more homogeneous with time. The high local thermal conductivity of both the SiC fabric and Al_2O_3 foam are the key driving force for this homogenisation. The level of uniformity and the heating rate appear to be a trade-off; the slower the heating process, the more uniform the temperature pattern at the upper end of the temperature range as expected.

The modelling results explicitly indicate that temperature distributions in the SiC preforms may be modulated by the control of reflections from the microwave system. However, the efficiency and precision of achieving such control in large microwave cavities appear to be problematic because of chaotic and indeterministic irradiation from the magnetron, the source of microwave power. The frequency spectra of magnetrons used in microwave power systems, as exemplified in [48-50], are very different and depend on many factors such as type of power supply used, load properties, temperature, the magnetron's physical construction, etc.

In practice, this intrinsic feature of magnetron generation of microwave power makes the use of special means for impedance matching (such as three- or four-stub waveguide tuners) mandatory in high-power microwave applicators. It also imposes certain objective limitations on full reproducibility of practical operations of magnetron-fed systems in computer models [30,41,48,50]. Special advanced techniques of modelling of typical magnetron excitations are discussed in [48,51]. However, these themes were not in the scope of the present study.

The objective of the modelling effort was to break down the complex process of MW CVI into multiple components to help analyse it, explain some experimental observations, and suggest a means of better control over the process. The model employed in this paper does not pretend to be comprehensive and fully represent the entire phenomenon that is a combination of multiple interacting electromagnetic, chemical and physical processes. This modelling study is focused on the interaction of the microwave field with the absorbing dielectric materials that is seen an underlying occurrence of MW CVI. The model does not consider any chemical reactions taking place in the preform or the change in density due to the deposition of the SiC matrix that likely affect the thermal and

dielectric properties of the materials involved in the microwave heating process. The model also does not consider the flow of gas into the preform, which will have had a cooling effect on the fibres. Rotation of the turntable carrying the quartz support with the preform was not accounted in the model. Neither were there attempts to imitate the pulsing microwave processing regime employed in the experimental production of the SiC_f/SiC composites due to the PID.

Nevertheless, the models developed seem to be capable of capturing the key features of the process of microwave heating of the materials used in the experiments. The observed effects of instability and unpredictability of the heating rates, substantial difficulties in reproducibility of experimental results, as well as other issues, received reasonable explanations and meaningful interpretations that are consistent with the experimental observations. For instance, in a series of visualisations made during typical microwave processing of the 55 × 8 mm SiC preforms, Fig. 19(a)-(c), a *hot spot* that was regularly formed 10 mm off-centre of the preform is evident. This was one of the issues with the ME CVI process, as the development of the *hot spot* led to the creation of a positive feedback loop; the hotter spot meant there were increased kinetics of the decomposition reaction, leading to higher density, which meant better microwave absorption and higher thermal conductivity, resulting in even higher temperatures with increasing ε' and ε'', and so on as the loop repeated. The ability to control this loop is fundamental to realising the potential of microwave processing in CVI. A similar pattern with the *hot spot* in the same off-centre location was obtained in the simulation, Fig. 19(d).

The computational study outlined in this paper eloquently illuminates the well-known observation that the magnetron-based processes of heating of small pieces of absorbing materials in large microwave cavities are naturally hard to control. The use of a solid-state generator can provide increasing flexibility in choosing (and, if necessary, alternating) the frequency of the thermal processing, the amplitude of the field, and hence in maintaining a desirable heating regimen [52]. Such a solid-state microwave generator is now installed on the ME CVI system at the University of Birmingham, UK.

Overall, this work has clearly highlighted the need and value of FDTD multiphysics modelling capabilities to support complex experimental studies in microwave power engineering. Without this tool research may not be sufficiently proactive in the design of experiments and the interpretation of experimental data may be limited. In the reported study, the EM and EM-thermal models of the microwave system have provided useful insight where experiments and measurement tools were lacking.

Declaration of Competing Interest

The authors declare the following financial interests/personal relationships which may be considered as potential competing interests: Matthew Porter reports financial support was provided by Airforce Office of Scientific Research.

Acknowledgements

This work was partially supported by the US Air Force Office of Scientific Research, Award FA9550–15-1–0465.

Appendix I

The functionality of the iterative procedure for solving the coupled EM-thermal problem in the microwave-induced heating processes [30–33] was explored with the model developed and employed in this study for computational characterisation of ME CVI production of SiC_f/SiC composites. The goal of the tests was to clarify how computational characterisation of time evolution of the heating process depends on the HTS $\Delta\tau$ pre-set in that iterative procedure. Two sets of the $T_{max}(t)$ curves generated in these computations are exemplified in Figs. 20 and 21.

It is seen that the time-temperature characteristics notably depend on $\Delta\tau$. The general perception (see Section 3.1) that the HTS should be sufficiently small to promote accurate upgrade of material parameters is eloquently confirmed. The curves seem to converge to those corresponding to the values $\Delta\tau = 0.2 – 0.5$ s and $\Delta\tau = 2 – 5$ s for the processes with high and low heating rates, respectively.

For the fastest heating scenario occurring with a constantly high energy coupling (frequency VII), the difference in determination of T_{max} at particular time instances with $\Delta\tau$ being 0.5 s and 5 s may reach 130 – 140 °C (or 30% error). Compared to frequency VII, at frequency I (when coupling worsens whilst heating), the heating rate was slightly lower, but the difference in maximum temperatures for those HTSs was reduced to 40 – 50 °C.

It is also seen that whilst a profile of a $T_{max}(t)$ curve seems not to change much with increase of the HTS, the accuracy in determination of temperature patterns may notably worsen. It is evident from Figs. 12–17 that in the process of microwave heating of SiC fabric discs characterised by high thermal conductivity, the patterns were substantially homogenised with time. Yet, for more precise reconstruction of the time-temperature history in terms of heat distributions, a choice of HTS corresponding to a converged $T_{max}(t)$ characteristic appears to be critical.

With further increase of $\Delta\tau$, the time-temperature characteristics may fall apart – such an effect is observed for the fastest heating scenario (frequency VII) with HTS being 8 s, Fig. 21; for the slower process (frequency I), Fig. 20, it is, however, less pronounced even for $\Delta\tau = 15$ s

These computational tests clearly illustrate the sensitivity of the simulation to the time-temperature history of the microwave heating processes by the FDTD-based iterative procedure for the EM-thermal coupled problem [30–33]. The computational cost of the simulation along the converged $T_{max}(t)$ curve is obviously higher, so future systematic studies of influence of the HTS on the accuracy and adequacy of the simulation should help resolve this inevitable trade-off in computational characterisation of microwave-induced temperature fields.

Appendix II

For the use of the FDTD EM simulator in the *QuickWave* computational environment containing *QW-BHM*, experimental data on EM and thermal material parameters (Section 3.2) were determined (through appropriate interpolation and approximation) for a set of particular temperatures that was made for more accurately representing non-linearity of the material parameters at high temperatures. Tables 5–7 contains corresponding values of.

dielectric constant, loss factor, specific heat and thermal conductivity for SiC fabric, alumina foam, and quartz respectively.

References

[1] V. Giurgiutiu, Structural health monitoring of aerospace composites, Struct. Heal. Monit. Aerosp. Compos (2015) 1–457, https://doi.org/10.1016/C2012-0-07213-4.
[2] A.R. Hyde, Ceramic matrix composites: high-performance materials for space application, Mater. Des. 14 (1993) 97–102, https://doi.org/10.1016/0261-3069(93)90002-D.
[3] R. Naslain, Design, preparation and properties of non-oxide CMCs for application in engines and nuclear reactors: An overview, Compos. Sci. Technol. 64 (2004) 155–170, https://doi.org/10.1016/S0266-3538(03)00230-6.
[4] X.W. Yin, L.F. Cheng, L.T. Zhang, N. Travitzky, P. Greil, Fibre-reinforced multifunctional SiC matrix composite materials, Int. Mater. Rev. 62 (2017) 117–172, https://doi.org/10.1080/09506608.2016.1213939.
[5] T. Aoki, T. Ogasawara, Tyranno ZMI fiber/TiSi2-Si matrix composites for high-temperature structural applications, Compos. Part A Appl. Sci. Manuf. 76 (2015) 102–109, https://doi.org/10.1016/j.compositesa.2015.05.018.
[6] J.D. Kiser, R.T. Bhatt, G.N. Morscher, H.M. Yun, J. a Dicarlo, J.F. Petko, SiC / SiC Ceramic Matrix Composites Developed for High-Temperature Space Transportation Applications, NASA Tech. Rep. Serv. - Res. Technol. 2004 (2006) 1–3. ⟨https://ntrs.nasa.gov/citations/20050217198⟩.
[7] O. Flores, R.K. Bordia, D. Nestler, W. Krenkel, G. Motz, Ceramic fibers based on SiC and SiCN systems: Current research, development, and commercial status, Adv. Eng. Mater. 16 (2014) 621–636, https://doi.org/10.1002/adem.201400069.

[8] M.-B. Coltelli, A. Lazzeri, Chem. Vap. infiltration Compos. their Appl. (2019), https://doi.org/10.1201/9781315117904-8.

[9] L.A. Timms, W. Westby, C. Prentice, D. Jaglin, R.A. Shatwell, J.G.P.P. Binner, Reducing chemical vapour infiltration time for ceramic matrix composites, J. Microsc. 201 (2001) 316–323, https://doi.org/10.1046/j.1365-2818.2001.00840.x.

[10] P.L.C. Rolls-Royce, Future Products, 2019. ⟨https://www.rolls-royce.com/products-and-services/civil-aerospace/future-products.aspx#/⟩.

[11] S. Tang, C. Hu, S, H. Tang C, Design, Preparation and properties of carbon fiber reinforced ultra-high temperature ceramic composites for aerospace applications: A Review, J. Mater. Sci. Technol. 33 (2017) 117–130, https://doi.org/10.1016/j.jmst.2016.08.004.

[12] L.C. Veitch, W.S. Hong, Will pigs fly before ceramics do? Ceram. Eng. Sci. Proc. 22 (2001) 31–37, https://doi.org/10.1002/9780470294680.ch4.

[13] J.A. DiCarlo, M. Van Roode, Ceram. Compos. Dev. Gas. Turbine Engine Hot Sect. Compon. (2006) 221–231, https://doi.org/10.1115/GT2006-90151.

[14] J. Binner, M. Porter, B. Baker, J. Zou, V. Venkatachalam, V.R. Diaz, A. D'Angio, P. Ramanujam, T. Zhang, T.S.R.C.S.R.C. Murthy, Selection, processing, properties and applications of ultra-high temperature ceramic matrix composites, UHTCMCs – a review, Int. Mater. Rev. (2019) 1–56, https://doi.org/10.1080/09506608.2019.1652006.

[15] A. Lazzeri, CVI Process. Ceram. Matrix Compos. (2012), https://doi.org/10.1002/9781118176665.ch9.

[16] D.J. Devlin, R.P. Currier, R.S. Barbero, B.F. Espinoza, N. Elliott, Microwave Assisted Chemical Vapor Infiltration, MRS Proc. 250 (1991), https://doi.org/10.1557/proc-250-245.

[17] D. Jaglin, J. Binner, B. Vaidhyanathan, C. Prentice, B. Shatwell, D. Grant, Microwave heated chemical vapor infiltration: Densification mechanism of SiCf/SiC composites, J. Am. Ceram. Soc. 89 (2006) 2710–2717, https://doi.org/10.1111/j.1551-2916.2006.01127.x.

[18] D.J. Devlin, R.P. Currier, J.R. Laia Jr, R.S. Barbero, Chemical vapor infiltration using microwave energy, (1993).

[19] M. Porter, High-Temperature Ceramic Matrix Composites Prepared via Microwave Energy Enhanced Chemical Vapour Infiltration, University of Birmingham,, 2020. ⟨https://etheses.bham.ac.uk/id/eprint/10629/⟩.

[20] M.T. Porter, A. D'Angio, J. Binner, M.K. Cinibulk, SiCf/SiC ceramic matrix composites using microwave enhanced chemical vapour infiltration, in: 56th IMPI's Microw. Power Symp., 2022: p. 3.

[21] B. Cioni, A. Lazzeri, Modeling and development of a microwave heated pilot plant for the production of SiC-based ceramic matrix composites, Int. J. Chem. React. Eng. 6 (2008), https://doi.org/10.2202/1542-6580.1562.

[22] K.I. Rybakov, E.A. Olevsky, E.V. Krikun, Microwave Sintering: Fundamentals and Modeling, J. Am. Ceram. Soc. 96 (2013) 1003–1020, https://doi.org/10.1111/jace.12278.

[23] D. Agrawal, 12 - Microwave sintering of metal powders, in: Y.B.T.-A. I. Chang, P. M. Zhao (Eds.), Woodhead Publ. Ser. Met. Surf. Eng., Woodhead Publishing, 2013, pp. 361–379, https://doi.org/10.1533/9780857098900.3.361.

[24] S. Sano, A. Tsuzuki, J. Li, A. Gotou, Y. Makino, S. Miyake, in: S.B.T.-N.M.P., A.E.E. S. Miyake (Eds.), Millimeter-wave dielectric measurement of SiC powders as a basis of millimeter-wave sintering of ceramics, Elsevier Science Ltd, Oxford, 2005, pp. 151–154, https://doi.org/10.1016/B978-008044504-5/50030-1.

[25] J. Binner, K. Annapoorani, A. Paul, I. Santacruz, B. Vaidhyanathan, Dense nanostructured zirconia by two stage conventional/hybrid microwave sintering, J. Eur. Ceram. Soc. 28 (2008) 973–977.

[26] T. Ibn-Mohammed, C.A. Randall, K.B. Mustapha, J. Guo, J. Walker, S. Berbano, S.C. L. Koh, D. Wang, D.C. Sinclair, I.M. Reaney, Decarbonising ceramic manufacturing: A techno-economic analysis of energy efficient sintering technologies in the functional materials sector, J. Eur. Ceram. Soc. 39 (2019) 5213–5235, https://doi.org/10.1016/j.jeurceramsoc.2019.08.011.

[27] T.E. Toolbox, Emissivity Coefficients Materials, (2003). ⟨https://www.engineeringtoolbox.com/emissivity-coefficients-d_447.html⟩.

[28] G. Galli, H. Hassen, J. C, K. Michael, O. Emmanuel, D. Philippe, M. Philippe, Paschen's Law in Extreme Pressure and Temperature Conditions, IEEE Trans. Plasma Sci. 47 (2019) 1641–1647.

[29] QuickWaveTM, 1998–2022, QWED Sp. z o. o., ⟨www.qwed.eu⟩.

[30] T.V. Koutchma, V.V. Yakovlev, Computer modeling of microwave heating processes for food preservation, Math. Anal, Food Process (2010) 625–657.

[31] V.V. Yakovlev, S.M. Allan, M.L. Fall, H.S. Shulman, Computational study of thermal runaway in microwave processing of zirconia, Microw. RF Power Appl. (2011) 303–306.

[32] P. Kopyt, M. Celuch, Coupled electromagnetic-thermodynamic simulations of microwave heating problems using the FDTD algorithm, J. Microw. Power Electromagn. Energy 41 (2007) 18–29. ⟨https://www.scopus.com/inward/record.uri?eid=2-s2.0-45549105452&partnerID=40&md5=131d652d90609c331d6dbfa3603d0c6c⟩.

[33] M. Celuch, P. Kopyt, Modeling microwave heating in foods, in: Dev. Packag. Prod. Use Microw. Ovens, Elsevier,, 2009, pp. 305–348.

[34] E.M. Kiley and V.V. Yakovlev, Modeling of microwave ovens with perforated metal walls, In: IEEE MTT-S Intern. Microwave Symp. Dig. (Baltimore, MD, June 2011), ⟨10.1109/MWSYM.2011.5972947⟩, pp. 1–4.

[35] I. Ghorbel, P. Gnaster, N. Moulin, C. Meunier, J. Bruchon, Experimental and numerical thermal analysis for direct microwave heating of silicon carbide, J. Am. Cer. Soc. (2020) 1–11, 10.111/jace.17451.

[36] J.M. Catalá-Civera, A.J. Canós, P. Plaza-González, J.D. Gutiérrez, B. García-Baños, F.L. Peñaranda-Foix, Dynamic measurement of dielectric properties of materials at high temperature during microwave heating in a dual mode cylindrical cavity, IEEE Trans. Microw. Theory Tech. 63 (2015) 2905–2914, https://doi.org/10.1109/TMTT.2015.2453263.

[37] N.R. Greenacre, Measurement of the high-temperature dielectric properties of ceramics at microwave frequencies, University of Nottingham,, 1996.

[38] H. Ichikawa, Polymer-Derived Ceramic Fibers, Annu. Rev. Mater. Res. 46 (2016) 335–356, https://doi.org/10.1146/annurev-matsci-070115-032127.

[39] PubChem, Alumina, Natl. Cent. Biotechnol. Inf. (2021). ⟨https://pubchem.ncbi.nlm.nih.gov/compound/Alumina⟩.

[40] ASTM, Standard Test Method for Thermal Diffusivity by the Flash Method, ASTM E1461–13. (2013). ⟨https://doi.org/10.1520/E1461–13⟩.

[41] V.A. Mechenova, V.V. Yakovlev, Efficiency optimization for systems and components in microwave power engineering, J. Microw. Power Electromagn. Energy 39 (1) (2004) 15–30.

[42] E. Murphy, V. Yakovlev, Neural Network Optimization of Complex Microwave Structures with a Reduced Number of Full-Wave Analyses, Int. J. RF Microw. Comput. Eng. 21 (2011) 279–287, https://doi.org/10.1002/mmce.20514.

[43] E. Murphy, V. Yakovlev, RBF network optimization of complex microwave systems represented by small FDTD modeling data sets, Microw. Theory Tech. IEEE Trans. 54 (2006) 3069–3083, https://doi.org/10.1109/TMTT.2006.877059.

[44] S. Tamang, S. Aravindan, 3D numerical modelling of microwave heating of SiC susceptor, Appl. Therm. Eng. 162 (2019), 114250, https://doi.org/10.1016/j.applthermaleng.2019.114250.

[45] R. D'Ambrosio, L. Aliotta, V. Gigante, M.B. Coltelli, G. Annino, A. Lazzeri, Design of a pilot-scale microwave heated chemical vapor infiltration plant: An innovative approach, J. Eur. Ceram. Soc. (2020) 0–1, https://doi.org/10.1016/j.jeurceramsoc.2020.05.073.

[46] G. Maizza, M. Longhin, Modelling of SiC Chemical Vapour Infiltration Process Assisted by Microwave Heating, in: COMSOL Conf., COMSOL, Milan, 2009.

[47] P. Kumi, V. Yakovlev, Computational procedure for quantitative characterization of uniformity of high frequency heating, Proc. 53rd IMPI's Microw. Power Symp. (2019).

[48] M. Celuch, W. Gwarek, M. Olszewska-Placha, Modeling of excitation in domestic microwave ovens, in: 2020: pp. 531–555. ⟨https://doi.org/10.1016/B978–0-08–102713-4.00020–7⟩.

[49] T.V.C.T. Chan, H.C. Reader, Understanding microwave heating cavities, Boston (Mass.), Artech house,, 2000. ⟨http://lib.ugent.be/catalog/rug01:000774672⟩.

[50] P. Kopyt, M. Celuch-Marcysiak, W.K. Gwarek, Microwave processing of temperature-dependent and rotating objects: development and experimental verification of FDTD algorithms, in: Microw. Radio Freq. Appl. Proceeding Third World Congr. Microw. Radio Freq. Appl., 2003: pp. 7–16.

[51] S.L. Birla, K. Pitchai, 18 - Simulation of microwave processes, in: M. Regier, K. Knoerzer, H.B.T.-T.M.P., F. Second, E. Schubert (Eds.), Woodhead Publ. Ser. Food Sci. Technol. Nutr., Woodhead Publishing, 2017, pp. 407–431, https://doi.org/10.1016/B978-0-08-100528-6.00018-8.

[52] V.V. Yakovlev, Effect of frequency alteration regimes on the heating patterns in a solid-state-fed microwave cavity, J. Microw. Power Electromagn. Energy 52 (2018) 31–44, https://doi.org/10.1080/08327823.2017.1417105.